iScience

CellPress
OPEN ACCESS

Article

Dual specificity kinase DYRK3 regulates cell migration by influencing the stability of protrusions

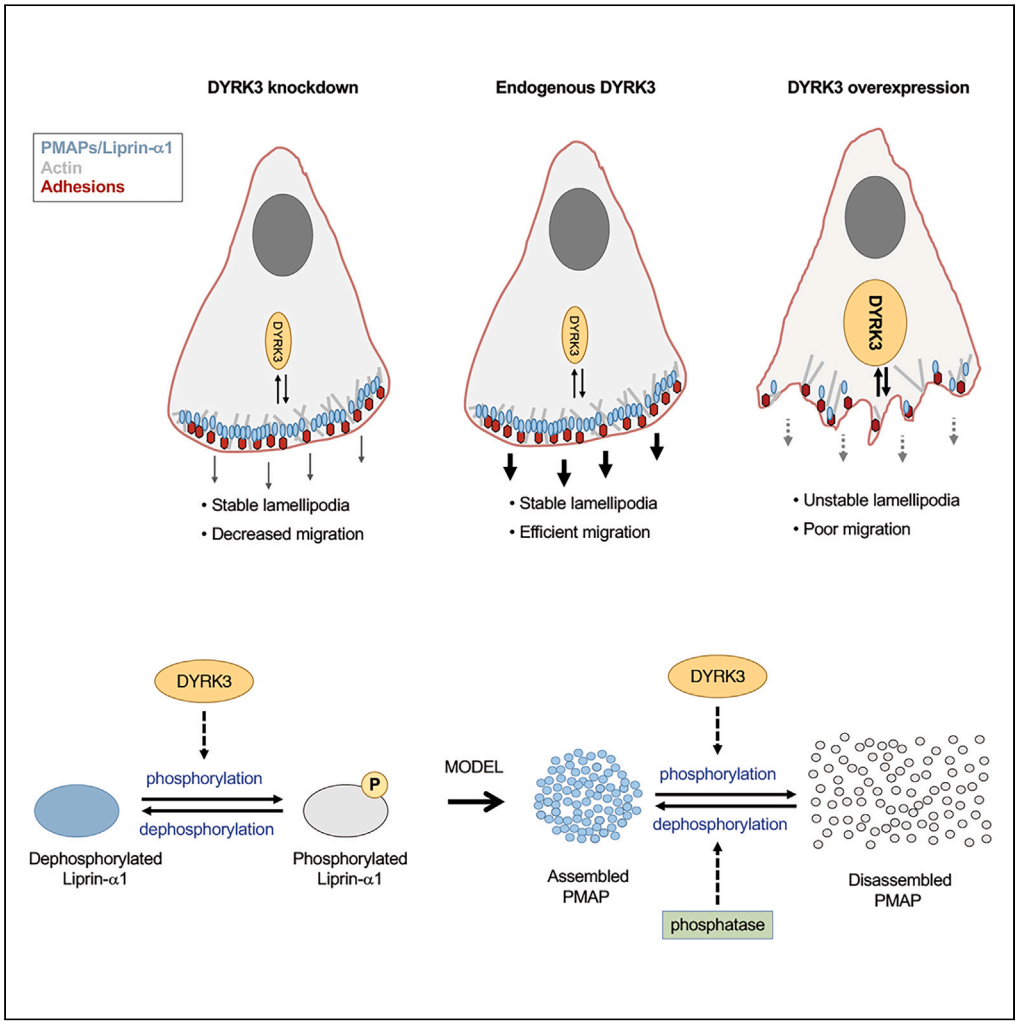

Martina Ramella, Lucrezia Maria Ribolla, Sara Surini, ..., Arpan Kumar Rai, Lucas Pelkmans, Ivan de Curtis

decurtis.ivan@hsr.it

Highlights

PMAPs are networks of scaffolds regulating cell motility by stabilizing lamellipodia

Ser/Thr kinase DYRK3 regulates migration and invasion of breast cancer cells

DYRK3 phosphorylates PMAP protein Liprin-α1 and affects lamellipodia stability

Balance between Liprin-α1 and DYRK3 levels is needed to sustain tumor cell motility

Ramella et al., iScience 27, 109440
April 19, 2024
https://doi.org/10.1016/j.isci.2024.109440

iScience

CellPress
OPEN ACCESS

Article

Dual specificity kinase DYRK3 regulates cell migration by influencing the stability of protrusions

Martina Ramella,[1,2] Lucrezia Maria Ribolla,[1,2] Sara Surini,[1,2] Kristyna Sala,[1,2] Diletta Tonoli,[2] Jean-Michel Cioni,[3] Arpan Kumar Rai,[4] Lucas Pelkmans,[4] and Ivan de Curtis[1,2,5,*]

SUMMARY

Plasma membrane-associated platforms (PMAPs) form at specific sites of plasma membrane by scaffolds including ERC1 and Liprin-α1. We identify a mechanism regulating PMAPs assembly, with consequences on motility/invasion. Silencing Ser/Thr kinase DYRK3 in invasive breast cancer cells inhibits their motility and invasive capacity. Similar effects on motility were observed by increasing DYRK3 levels, while kinase-dead DYRK3 had limited effects. DYRK3 overexpression inhibits PMAPs formation and has negative effects on stability of lamellipodia and adhesions in migrating cells. Liprin-α1 depletion results in unstable lamellipodia and impaired cell motility. DYRK3 causes increased Liprin-α1 phosphorylation. Increasing levels of Liprin-α1 rescue the inhibitory effects of DYRK3 on cell spreading, suggesting that an equilibrium between Liprin-α1 and DYRK3 levels is required for lamellipodia stability and tumor cell motility. Our results show that DYRK3 is relevant to tumor cell motility, and identify a PMAP target of the kinase, highlighting a new mechanism regulating cell edge dynamics.

INTRODUCTION

Cell migration on extracellular matrix (ECM) requires continuous dynamic rearrangements of the protruding cell edge, where actin dynamics and integrin-mediated focal adhesions contribute to the protrusive activity of cells.[1,2] Plasma membrane-associated platforms (PMAPs) are formed by the dynamic assembly of a network of scaffold proteins at specific sites of the cell membrane,[3,4] including the cortex of non-motile cells,[5,6] or near integrin-mediated focal adhesions and invadosomes at the front of motile cells to sustain migration.[7–10] Liprins are a family of scaffold proteins[11] playing important functions in the organization of neuronal synapses[12–14] and in cellular processes relevant to cancer progression.[15] We have previously shown that the PMAP scaffold protein Liprin-α1 enhances cell spreading and has a stabilizing effect on the lamellipodia, while depletion of endogenous Liprin-α1 results in the formation of unstable lamellipodia and strongly impaired cell spreading and motility.[8,16,17] The mechanisms regulating PMAP constituents including Liprin-α1, and the formation and turnover of PMAPs are unknown. The mammalian dual-specificity tyrosine (Y) phosphorylation–regulated kinase (DYRK) family includes kinases that share a conserved kinase and N-terminal DYRK homology domain (DH-box), while they differ in N- and C- terminal extensions. The term dual kinase refers to the fact that DYRK proteins autophosphorylate on one specific residue of tyrosine within the activation loop to get fully activated. Autophosphorylation of tyrosine residues in the activation loop is essential for their Ser/Thr kinase activity. The specificity for tyrosines is then lost, and kinase activity becomes restricted to threonine and serine residues.[18]

DYRKs are divided into two subgroups: class I kinases including DYRK1A and DYRK1B show a predominant nuclear localization, while class II kinases including DYRK2, DYRK3, and DYRK4 have a predominant cytoplasmic localization.[19–21] In this study, we investigated the molecular mechanisms that regulate motility during tumor cell migration, and found that the DYRK3 kinase is required for the formation of PMAPs and for efficient cell motility. Altering DYRK3 levels in cells influences the stability of lamellipodia at the cell edge, as observed after Liprin-α1 depletion. Our findings also identify Liprin-α1 as a substrate of DYRK3, and suggest that an equilibrium between Liprin-α1 and DYRK3 levels is required for the stabilization of lamellipodia and efficient tumor cell motility.

[1]Università Vita-Salute San Raffaele, 20132 Milan, Italy
[2]Cell Adhesion Unit, Division of Neuroscience, IRCCS San Raffaele Scientific Institute, 20132 Milan, Italy
[3]RNA Biology of the Neuron Unit, Division of Neuroscience, IRCCS San Raffaele Scientific Institute, 20132 Milan, Italy
[4]Department of Molecular Life Sciences, University of Zurich, 8057 Zurich, Switzerland
[5]Lead contact
*Correspondence: decurtis.ivan@hsr.it
https://doi.org/10.1016/j.isci.2024.109440

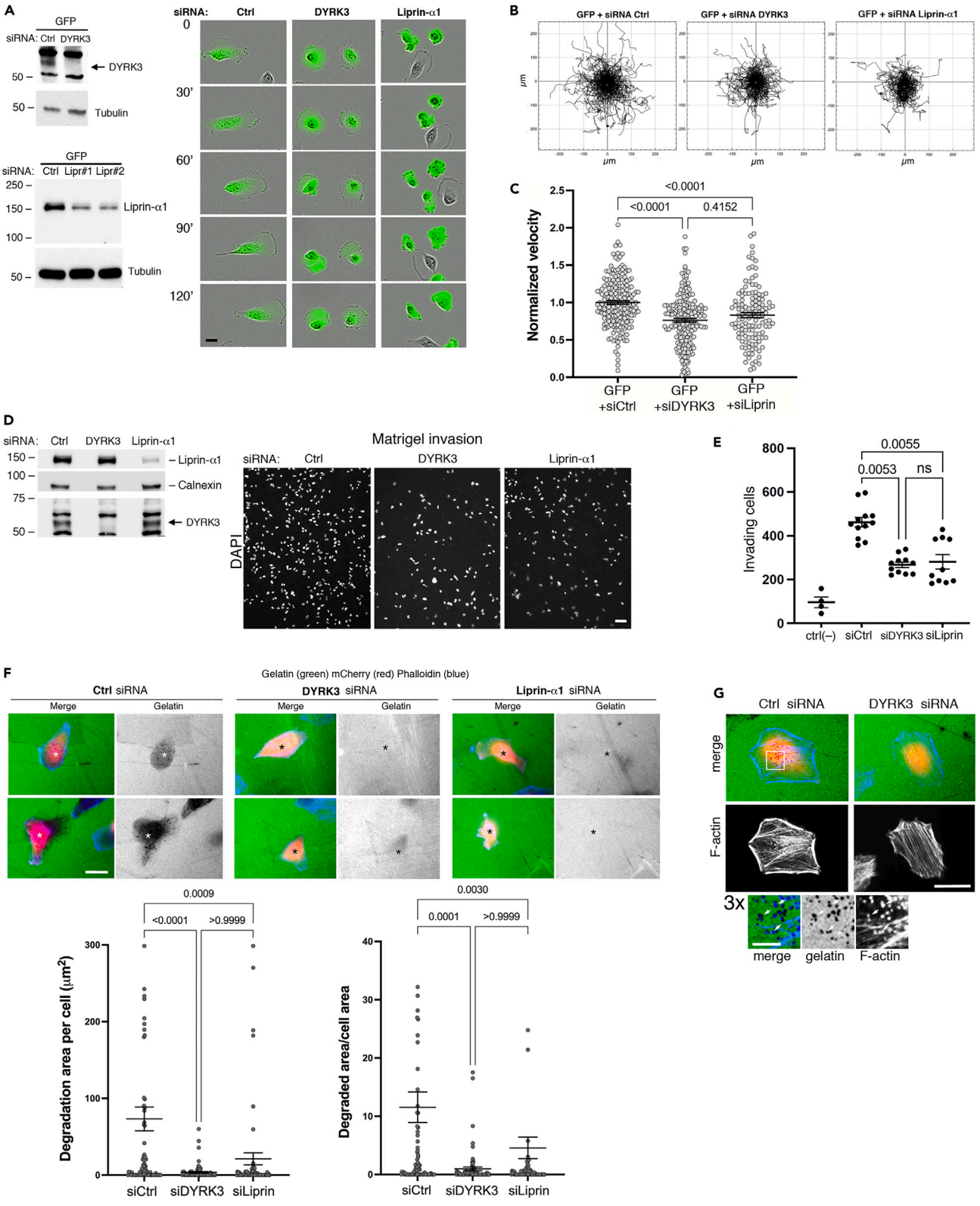
A
GFP
siRNA: Ctrl DYRK3
DYRK3
Tubulin
siRNA: Ctrl Lipr#1 Lipr#2
Liprin-α1
Tubulin
siRNA: Ctrl DYRK3 Liprin-α1
0
30'
60'
90'
120'
B
GFP + siRNA Ctrl
GFP + siRNA DYRK3
GFP + siRNA Liprin-α1
μm
C
Normalized velocity
<0.0001
<0.0001
0.4152
GFP +siCtrl
GFP +siDYRK3
GFP +siLiprin
D
siRNA: Ctrl DYRK3 Liprin-α1
Liprin-α1
Calnexin
DYRK3
Matrigel invasion
siRNA: Ctrl DYRK3 Liprin-α1
DAPI
E
Invading cells
0.0055
0.0053
ns
ctrl(–) siCtrl siDYRK3 siLiprin
F
Gelatin (green) mCherry (red) Phalloidin (blue)
Ctrl siRNA
DYRK3 siRNA
Liprin-α1 siRNA
Merge
Gelatin
Degradation area per cell (μm²)
0.0009
<0.0001
>0.9999
Degraded area/cell area
0.0030
0.0001
>0.9999
siCtrl siDYRK3 siLiprin
G
Ctrl siRNA
DYRK3 siRNA
merge
F-actin
3x
merge gelatin F-actin

Figure 1. Silencing of endogenous DYRK3 inhibits tumor cell motility

(A) Left: efficient silencing of endogenous DYRK3 and endogenous Liprin-α1 by immunoblotting on 50 μg of protein lysate per lane. Right: frames from time-lapses of GFP–positive control, DYRK3–silenced, and Liprin-α1–silenced MDA-MB-231 cells migrating on fibronectin. Bar, 20 μm.

(B) Plots with tracks of migrating GFP–positive cells cotransfected with the indicated siRNAs, and (C) normalized velocity (to GFP + siRNA Ctrl) with means ± SEM (n = 125–204 cells, 3/4 experiments). Statistical analysis: Kruskal-Wallis test with Dunn's posthoc.

(D) Inhibition of transwell Matrigel invasion by MDA-MB-231 cells (right) after silencing of either DYRK3 or Liprin-α1 (left). Bar, 50 μm.

(E) Quantification of invading cells (means ± SEM; n = 10–12 wells/siRNA, 4 experiments). To stimulate invasion, lower chambers were filled with NIH 3T3-conditioned medium (+stimulus), while in control samples (ctrl(−) = no stimulus) lower chambers were filled with unconditioned medium. Statistical analysis: Kruskal-Wallis test with Dunn's posthoc; posthoc.

(F) Silencing of DYRK3 inhibits ECM degradation. MDA-MB-231 cells co-transfected with the indicated siRNAs and mCherry, were re-plated on coverslips coated with fluorescent gelatin and fibronectin. Top: after 5 h at 37°C cells were fixed and stained with fluorescent phalloidin. Asterisks indicate the position of transfected mCherry-positive cells. Bar, 20 μm. Bottom, left graph: quantification (with means ± SEM) of the dark areas of gelatin degradation; right graph, gelatin degradation corrected for the projected area of mCherry–positive cells (n = 75–85 cells per condition, 2 experiments; 8 and 13 data points fall outside the y axis limits of the left and right graph, respectively; these data points were included in the statistical analysis: Kruskal-Wallis test with Dunn's posthoc). Bar, 20 μm.

(G) F-actin–positive invadopodia. Left: micrograph of control and DYRK3–silenced cells (mCherry) on FITC-gelatin (green); F-actin-positive invadopodia are revealed by phalloidin staining (blue). Below: 3-fold enlargement of the area (white square). Arrowheads point to sites of colocalization of F-actin–rich invadopodia with areas of gelatin degradation. Bar, 20 μm (3x enlargement: bar, 5 μm).

RESULTS

Altering the levels of DYRK3 inhibits tumor cell motility and invasion

With the aim of identifying class II DYRK family members (DYRK2, DYRK3, and DYRK4) relevant for cell motility, we carefully tested a number of commercially available antibodies to identify suitable tools for the analysis of the endogenous proteins. This analysis revealed that a number of antibodies presented as specific for either DYRK3 or DYRK2 gave non-specific signals and recognized bands close to the expected molecular weight of the endogenous proteins. We found that specific detection of endogenous DYRK3 was achieved using a goat pAb (Novus Biologicals), that revealed the expression of the DYRK3 protein in COS7 and MDA-MB-231 breast cancer cells, but not in MCF7, T47D, and BT-474 breast cancer cells (Figure S1A). This antibody was specific for DYRK3 versus DYRK2, a closely related member of the DYRK family, as revealed by immunoblotting on filters with lysates from cells overexpressing either GFP-DYRK3 or GFP-DYRK2 (Figure S1C). We tested the expression of endogenous DYRK2 by immunoblotting with anti-DYRK2 Ab. Although low levels of endogenous DYRK2 were previously reported in MDA-MB-231 cells,[22] by testing commercial anti-DYRK2 antibodies recognizing the transfected GFP-DYRK2 protein, endogenous DYRK2 was virtually undetectable in MDA-MB-231 invasive breast cancer cells, while this kinase was detectable in COS7 and MCF7 breast cancer cells (Figure S1B). The specificity of the anti-DYRK2 Ab was shown by the disappearance of the band corresponding to either endogenous DYRK2 or overexpressed GFP-DYRK2 after transfection of DYRK2–specific siRNAs (Figure S1G). Moreover, by using a pool of three siRNAs specific for DYRK3,[23] we observed the efficient silencing of both overexpressed (Figure S1D) and endogenous (Figure S1E) DYRK3 protein in MDA-MB-231 cells. Finally, DYRK4 was not detected in MDA-MB-231 cells by a DYRK4-specific Ab recognizing both overexpressed GFP-DYRK4 and an endogenous band corresponding to the expected size for DYRK4 in COS7 cells (Figure S1F). Therefore, we conclude that MDA-MB-231 cells specifically express detectable levels of endogenous DYRK3, which was further investigated for its role in the motility of these cells.

We evaluated the effects of DYRK3 on tumor cell motility by analyzing the effects of altering its expression on the migration and invasion of human breast cancer MDA-MB-231 cells. Silencing of endogenous DYRK3 inhibited random cell migration on fibronectin (Figures 1A–1C), and caused a strong reduction of cell invasion *in vitro*, as observed after Liprin-α1 silencing (Figures 1D and 1E). The stronger inhibitory effect observed on the migration through the 3D environment of the thick layer of Matrigel compared to the limited inhibition observed on 2D migration may be due to the more challenging environment met by tumor cells in the 3D ECM. Invasive tumor cells may use the extension of lamellipodia together with ECM degradation to move through 3D challenging environments. We tested whether the strong inhibition of invasion after DYRK3 silencing was due also to a defect in ECM degradation. Indeed, silencing of DYRK3 inhibited ECM degradation by MDA-MB-231 cells (Figures 1F and 1G). Similar inhibitory effects were observed when endogenous DYRK3 was silenced in MDA-MB-231 cells expressing the constitutively active mutant SrcY527F tyrosine kinase that is known to potentiate the formation of invadopodia and the degrading capacity of these cells (Figures S2A and S2B).

We next tested the effects of increasing the levels of DYRK3 on tumor cell motility. Interestingly, MDA-MB-231 random cell migration on fibronectin was strongly inhibited by overexpressing GFP-DYRK3, and also by the kinase-dead mutant GFP-DYRK3^{K218M} (Figures 2A and 2B), although the inhibitory effect of this mutant was significantly weaker compared to the wild type kinase (Figure 2B). Although the effects on cell shape and motility were not as strong in cells overexpressing the kinase-dead mutant GFP-DYRK3^{K218M}, the results indicate that the inhibitory effects on tumor cell motility observed by increasing the levels of DYRK3 are partially kinase–independent. DYRK3 overexpression did also inhibit ECM degradation by MDA-MB-231 expressing the constitutively active mutant SrcY527F tyrosine kinase that potentiates the formation of invadopodia and the degrading capacity of these cells (Figure 2C). In absence of SrcY527F, MDA-MB-231 cells overexpressing Liprin-α1 showed significantly increased ECM degradation, while cells with DYRK3 overexpression showed only a non-significant trend ($p = 0.097$) toward decreased ECM degradation (Figure S3).

In addition of being poorly motile, cells expressing high levels of GFP-DYRK3 were poorly spread when plated on fibronectin-coated substrates (Figures S4A and S4B). The GFP-DYRK3–expressing cells appeared to be able to still form F-actin–rich lamellipodia (Figure S4C), suggesting that the edge of the cells is dynamic.

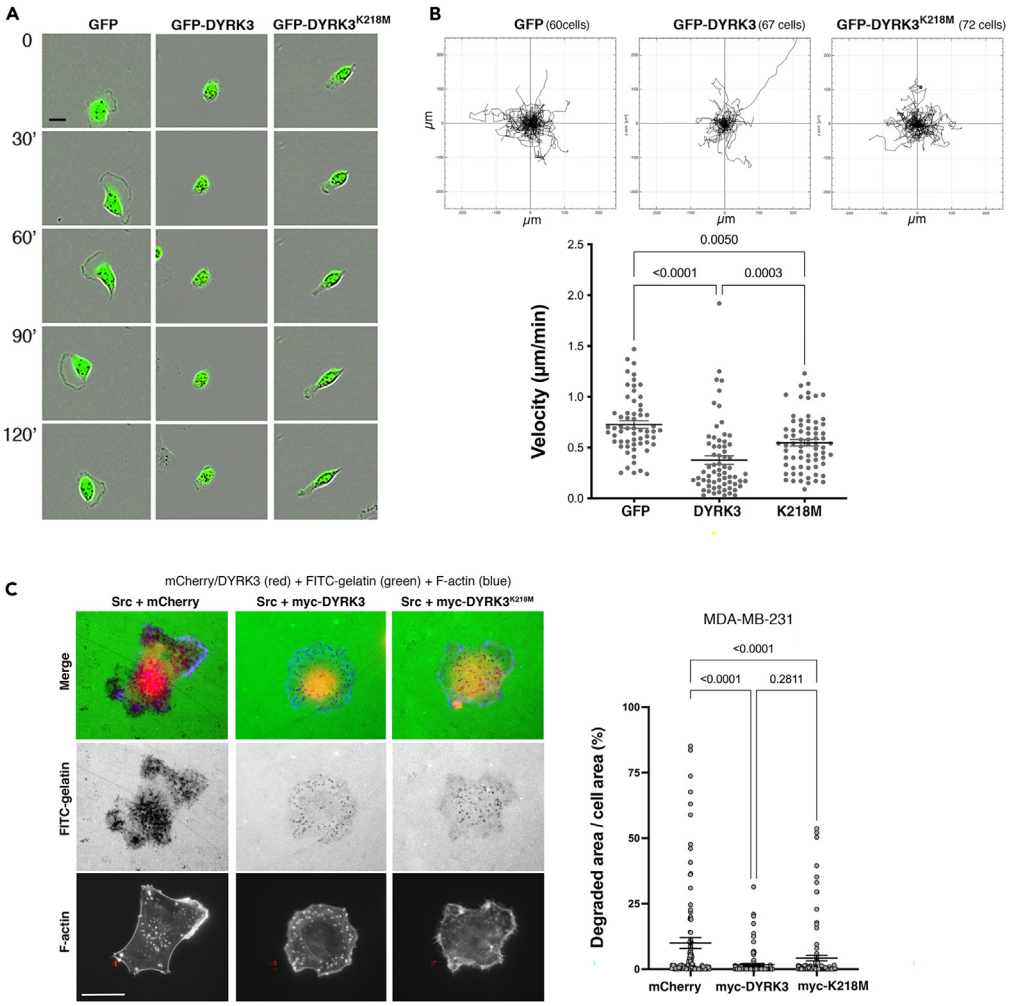

Figure 2. Increased levels of DYRK3 inhibit cell motility and ECM degradation

(A) Frames from time lapses of migrating MDA-MB-231 cells expressing the indicated constructs. Overexpression of GFP-DYRK3 decreases the speed of migration. Bar, 20 µm.

(B) Plots with tracks of GFP– or GFP-DYRK3–expressing cells migrating on fibronectin–coated substrates (4.5 h). Bars are means ± SEM (n = 60–72 cells from 3 to 4 experiments). Statistics: Kruskal-Wallis, Dunn's posthoc.

(C) MDA-MB-231 cells cotransfected with SrcY527F and either the indicated Myc-tagged constructs or mCherry (control) were re-plated on coverslips coated with FITC-gelatin and fibronectin. After 5 h at 37°C cells were fixed and stained to reveal the indicated proteins: Myc-DYRK3 (anti-DYRK3 Ab, red) and F-actin (phalloidin, blue). Bar, 20 µm. Graph: the dark areas of gelatin degradation and the projected areas of mCherry–positive cells were quantified on thresholded images by ImageJ. Bars are means ± SEM; n = 103–118 MDA-MB-231 cells from 2 experiments (1 point of mCherry transfected cells falls outside the shown y axis limit). Statistics: Kruskal-Wallis test with Dunn's posthoc.

Integrin–mediated cell spreading on ECM proteins is also used to address cell motility in poorly motile COS7 cells. We observed a significant decrease also of the projected area of COS7 cells spreading for 1 h on fibronectin after expression of either GFP-DYRK3 or GFP-DYRK2, but not by GFP-DYRK4 nor by the kinase inactive GFP-DYRK3^{K218M} protein (Figure S5).

Increased expression of DYRK3 perturbs the localization of PMAP proteins and focal adhesions at the protrusive edge of migrating MDA-MB-231 cells

How does DYRK3 influence tumor cell motility? Cell migration and invasion of MDA-MB-231 cells is supported by the interacting scaffold proteins ERC1 and Liprin-α1 that assemble into dynamic plasma membrane–associated platforms (PMAPs) forming near the protruding edge of motile normal[16] and tumor cells.[8] PMAPs assemble near integrin–mediated focal adhesions, and the PMAP core proteins ERC1 and Liprin-α1 have been shown to control tumor cell edge dynamics by promoting focal adhesion turnover.[24] On the other hand, DYRK3 has been shown to act as a dissolvase driving the disassembly of different types of membraneless organelles including stress granules, P granules and splicing speckles.[23,25,26] PMAPs are very dynamic and their assembly in tumor cells correlates with the extension of lamellipodia, while they

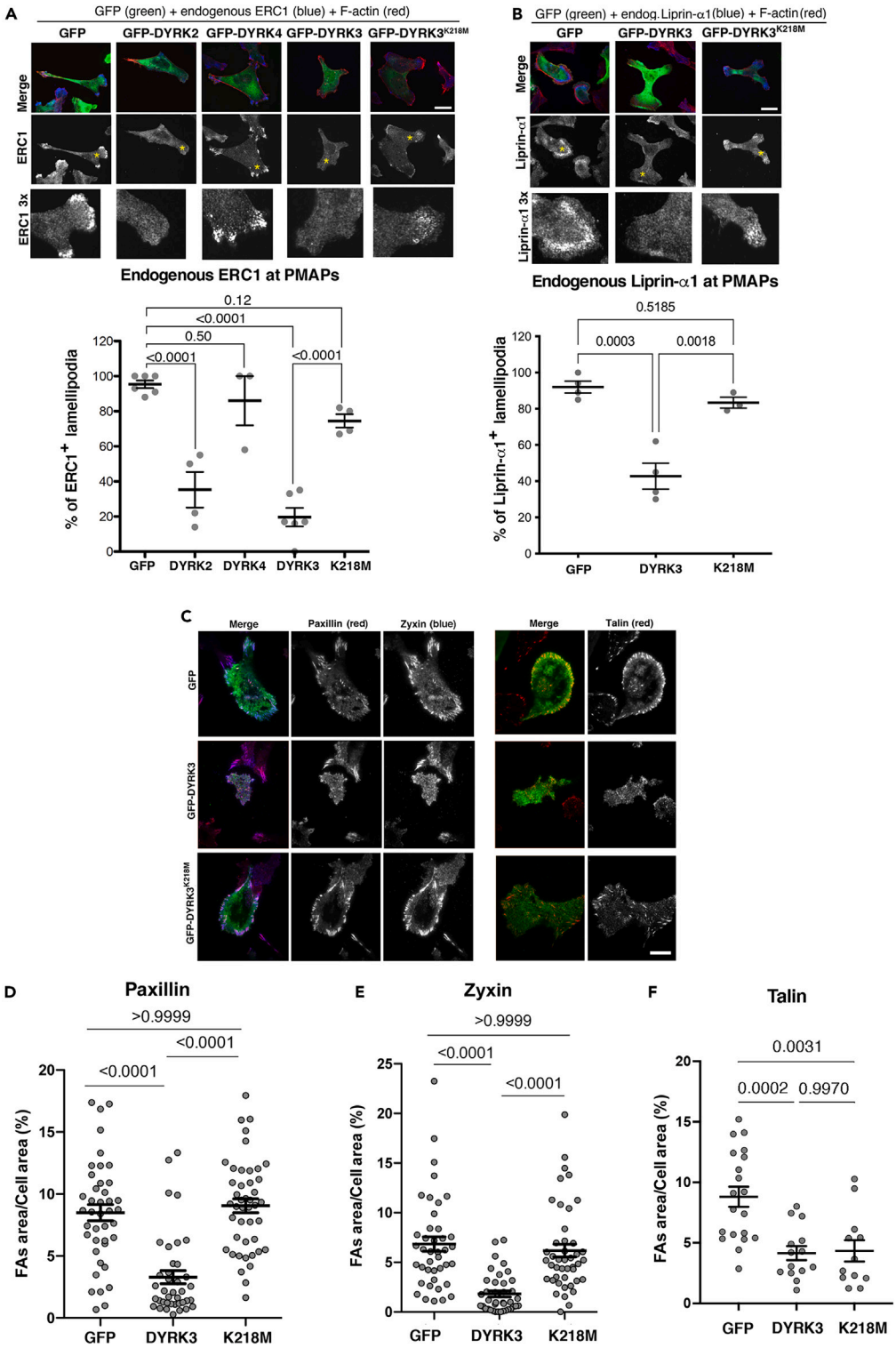

Figure 3. DYRK3 perturbs PMAPs and focal adhesions in migrating MDA-MB-231 cells

Confocal immunofluorescence showing the subcellular localization of endogenous proteins (blue) ERC1 (A), Liprin-α1 (B), and F-actin (red) in MDA-MB-231 cells transfected with the indicated GFP-tagged proteins (green). The yellow asterisks on the images of the middle rows (showing endogenous ERC1 in the left panel, and endogenous Liprin-α1 in the right panel) mark the lamellipodia enlarged in the corresponding higher magnifications shown in the respective bottom rows. Overexpression of either GFP-DYRK2 or GFP-DYRK3, but not of the kinase-dead mutant GFP-DYRK3^{K218M} nor of GFP-DYRK4, inhibits the accumulation of

Figure 3. *Continued*

endogenous ERC1 and Liprin-α1 at PMAPs in migrating cells. Graphs: means ± SEM of the percentage of lamellipodia with ERC1–positive PMAPs (n = 3–6 experiments) (A), and Liprin-α1–positive PMAPs (n = 3–4 experiments) (B). Each point represents the percentage of PMAP-positive lamellipodia measured in several cells for each experimental condition. Bars, 20 μm.

(C) TIRF microscopy of MDA-MB-231 cells cotransfected with GFP, GFP-DYRK3, or GFP-DYRK3^{K218M}. Fixed transfected cells (green, GFP) were immunostained for endogenous paxillin (red) and zyxin (blue) (left panel), or for endogenous talin (red, right panel). Bar, 10 μm.

(D–F) Quantification of the percentage of cell area occupied by focal adhesions (FA area/cell area) estimated for endogenous paxillin (D), endogenous zyxin (E), and endogenous talin (F); n = 39–44 cells per experimental condition for paxillin and zyxin (3 experiments); n = 12–20 cells for talin (2 experiments). Statistics: Kruskal-Wallis test with Dunn's posthoc (paxillin and zyxin); Brown-Forsythe and Welch ANOVA test with Dunnett's T3 posthoc (talin).

disassemble rapidly as cell advancement halts.[8] They may therefore be considered as highly dynamic biomolecular condensates functioning to support cell motility. Given the effects of DYRK3 on tumor cell motility, we investigated the effects of this kinase on PMAPs and focal adhesions in migrating cells. Expression of GFP-DYRK3 strongly inhibited the accumulation of the endogenous ERC1 (Figure 3A) and Liprin-α1 (Figure 3B) at PMAPs near the protruding edge of migrating MDA-MB-231 cells. Expression of GFP-DYRK2 caused similar effects and disappearance of ERC1-positive PMAPs, while these effects were not observed by expressing either the kinase-dead mutant GFP-DYRK3^{K218M} [25] or GFP-DYRK4 (Figure 3A). As mentioned earlier, MDA-MB-231 cells express detectable levels of endogenous DYRK3 (Figure S1A), while its closest family member DYRK2 was undetectable (Figure S1B). Silencing of endogenous DYRK3, although strongly affecting cell motility (Figure 1), did not affect the formation of dynamic ERC1–positive PMAPs in migrating MDA-MB-231 cells: migrating MDA-MB-231 cells silenced for endogenous DYRK3 and co-expressing GFP-ERC1 with RFP-LifeAct formed dynamic ERC1–positive PMAPs near lamellipodia, similar to those observed in cells transfected with control siRNA (Figure S6A). Moreover, quantification by confocal microscopy on fixed migrating MDA-MB-231 cells showed that silencing DYRK3 did not affect the localization of either ERC1 or Liprin-α1 at PMAPs near lamellipodia (Figures S6B and S6C).

We described that altering the expression of DYRK3 perturbs migration and invasion of tumor cells (Figures 1 and 2). Dynamics of integrin–mediated focal adhesions are important at the front of cells migrating on ECM. Liprin-α1 and other components of the PMAPs are known to affect integrin-mediated focal adhesions in migrating cells.[8,9] Given the strong effects of the increased expression of DYRK3 on the formation of PMAPs, we tested the effects of this kinase on the formation of focal adhesions in MDA-MB-231 cells migrating on fibronectin. Silencing endogenous DYRK3 did not evidently affect the distribution and presence of focal adhesions in MDA-MB-231 cells migrating on fibronectin, as detected by immunostaining and total internal reflection fluorescence (TIRF) microscopy with antibodies specific for zyxin and phosphotyrosine (Figure S7A). On the other hand, we observed a strong effect of the overexpression of DYRK3 on focal adhesions in MDA-MB-231 cells migrating on fibronectin. Focal adhesions were analyzed by considering three of their components: paxillin and talin found in the plasma membrane-proximal integrin signaling layer, and zyxin localized in the actin regulatory layer of focal adhesions.[27] Cells expressing GFP-DYRK3 were defective in paxillin- and zyxin-positive focal adhesions compared to cells expressing either GFP, DYRK4, or the kinase-dead mutant DYRK3^{K218M} (Figure 3C; Figures S7B and S7C). Analysis by TIRF microscopy confirmed the kinase-dependent strong reduction of the total focal adhesion area/cell area detected by immunostaining for both paxillin and zyxin in cells expressing GFP-DYRK3 compared to cells expressing either the kinase-dead mutant GFP-DYRK3^{K218M} or GFP (Figures 3D and 3E); intriguingly, talin was affected both by either kinase active or inactive DYRK3 (Figure 3F). The results indicate that the strong negative effects of DYRK3 on focal adhesions are kinase–dependent for paxillin and zyxin, while the membrane-proximal focal adhesion component talin is affected also by the kinase-dead DYRK3 mutant. Together these data suggest that the defects in the formation of PMAPs and focal adhesions may underlie the defect in migration observed after increasing the kinase activity of DYRK3.

To test if the effects on PMAPs and focal adhesions induced by altering the levels of DYRK3 could be observed in other cell types, we looked at the consequences of the overexpression of different DYRK proteins in COS7 cells. We analyzed the effects of DYRKs on focal adhesions in spreading COS7 cells. The expression of GFP-DYRK3 affected the distribution of focal adhesions in spreading COS7 cells in a kinase-independent manner: the density of small peripheral adhesions in spreading cells as well as central mature FAs were decreased (Figures 4A and 4B). The density of focal adhesions at the cell periphery and the number of central focal adhesions/cell were decreased by GFP-DYRK3 or GFP-DYRK3^{K218M}, but not by GFP-DYRK4 (Figures 4C and 4D). In COS7 cells endogenous ERC1 and Liprin-α1 accumulate at PMAPs near mature central focal adhesions and near fast-turning small adhesion complexes at the periphery of the spreading cell.[16] Given the link between PMAPs and focal adhesion dynamics,[8,9,24,28] selected areas including central focal adhesions and associated PMAPs were analyzed for the accumulation of endogenous PMAP proteins (ERC1 and Liprin-α1). Interestingly, in COS7 cells spreading on fibronectin the catalytically active kinase inhibiting spreading (Figure S5; Figures 4A and 4B) disrupted the organization of PMAPs around focal adhesions (Figure 4E), while kinase-dead DYRK3^{K218M} or the other family member DYRK4 affected neither spreading (Figure S5; Figures 4A and 4B), nor PMAPs accumulation around central adhesions (Figure 4E).

Increased DYRK3 expression perturbs cell edge dynamics and focal adhesion turnover

We next set to analyze the dynamics of lamellipodia in motile MDA-MB-231 cells co-transfected with mCherry-Zyxin to also compare the behavior of focal adhesions in cells with increased levels of DYRK3 (GFP-DYRK3) and in control cells (GFP). We observed a dramatic effect of the expression of DYRK3 on the behavior of the edge of MDA-MB-231 cells migrating on fibronectin: while lamellipodia were generally stable in control GFP-positive cells, several short-lived protrusions were observed in cells expressing wildtype GFP-DYRK3 (Videos S1 and S2; Figure 5A). The dynamics of the cell edge was evaluated on kymographs to measure different parameters (Figure 5B). DYRK3

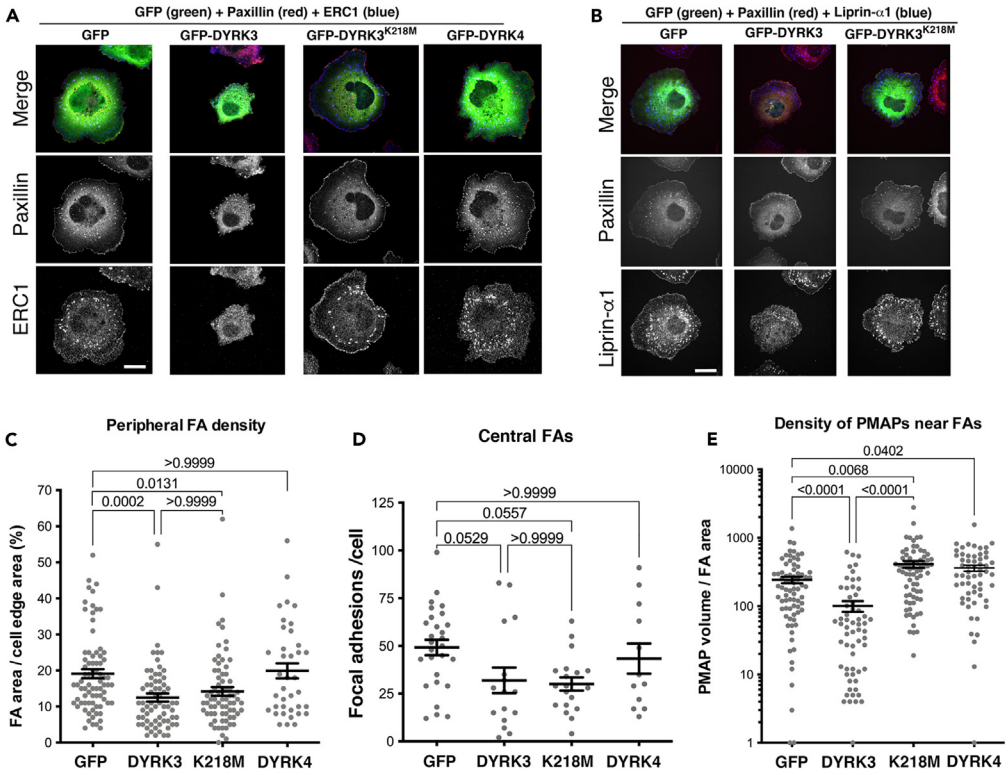

Figure 4. GFP-DYRK3 affects COS7 cell spreading and PMAPs localization at focal adhesions

COS7 cells expressing the indicated GFP-tagged proteins were allowed to spread for 1 h on fibronectin–coated substrate (10 μg/mL).

(A and B) Morphology of transfected cells (GFP, green) immunostained for endogenous paxillin (red) and PMAP components (ERC1 and Liprin-α1, blue). Bars, 20 μm.

(C) Graph bars represent mean percentage ± SEM of area occupied by focal adhesions within one μm–wide cell edge regions.

(D) Graph bars are means ± SEM of the number of central focal adhesions (obtained by excluding from the quantification the peripheral focal adhesions in the external 2.5 μm–wide cell edge. C: n = 77 (GFP), 67 (GFP-DYRK3), 72 (GFP-DYRK3^{K218M}) cell edges from two experiments. D: n = 28 (GFP), 16 (GFP-DYRK3), 19 (GFP-DYRK3^{K218M}) cells, from two experiments.

(E) Expression of DYRKs perturbs the formation of PMAPs near focal adhesions in spreading COS7 cells. Graph bars represent the normalized mean density ± SEM of endogenous ERC1–positive PMAPs (ratio ERC1 volume/FA area); n = 36–38 selected regions. Statistics: Kruskal-Wallis test with Dunn's posthoc.

overexpression resulted in a dramatic decrease in cell migration detected as the total displacement of the cell front during the 50 min time-lapse (Figure 5C). Quantitative analysis of single events of cell edge extension and retraction performed by analyzing kymographs at the dynamic cell border showed that the frequency of both events was significantly higher in GFP-DYRK3-positive cells compared to control GFP-positive cells (Figures 5D–5F). Analysis of single cell edge extension events during the 50 min recordings highlighted a large difference in terms of displacement between GFP cells and GFP-DYRK3 cells (Figure 5G, left graph); on the other hand, the average speed of cell edge extension (ratio between displacement and duration of the event) showed no significant difference (Figure 5G, right graph). These results suggest that the increased DYRK3 kinase activity does not alter the capacity of the cell to form protrusions, nor the machinery required to support the speed of their extension, while the persistence and stability of the protrusions is affected compared to control cells. Indeed, protrusions were highly unstable in cells with increased expression of the kinase, with numerous retraction events that were more rarely observed in control cells (Figure 5F). Interestingly, while the cell edge displacement was strongly reduced, the speed of cell edge extension was not affected in cells expressing DYRK3 compared to control GFP-expressing cells (Figure 5G). On the other hand, retraction events were much more frequent and occurred with higher speed in cells expressing GFP-DYRK3 compared to control cells (GFP). This different behavior results in the poorly effective migration observed for cells expressing GFP-DYRK3 (Figure 2).

Focal adhesions at the border of dynamic cells are turning rapidly to sustain cell motility, while focal adhesions placed at the center of the cell are more stable over time.[29] We measured the lifetime of mCherry-Zyxin–positive adhesions at protruding cell edges as described,[8,30] to check for differences between endogenous and increased DYRK3 expression. GFP-DYRK3 expression resulted in a significant decrease of the lifetime of newly formed zyxin-positive focal adhesions in migrating MDA-MB-231 cells (2.0 ± 0.1 min SEM; n = 394 FAs from 5 cells) compared to GFP expressing cells (3.4 ± 0.3 min SEM; n = 335 FAs from 5 cells) (Figures 5H and 5I). Together, the results show that increased expression of the DYRK3 kinase affects cell edge dynamics in motile cells: while the protrusive activity *per se* does not appear to be affected by the kinase, DYRK3 has a strong effect on the stabilization of lamellipodia.

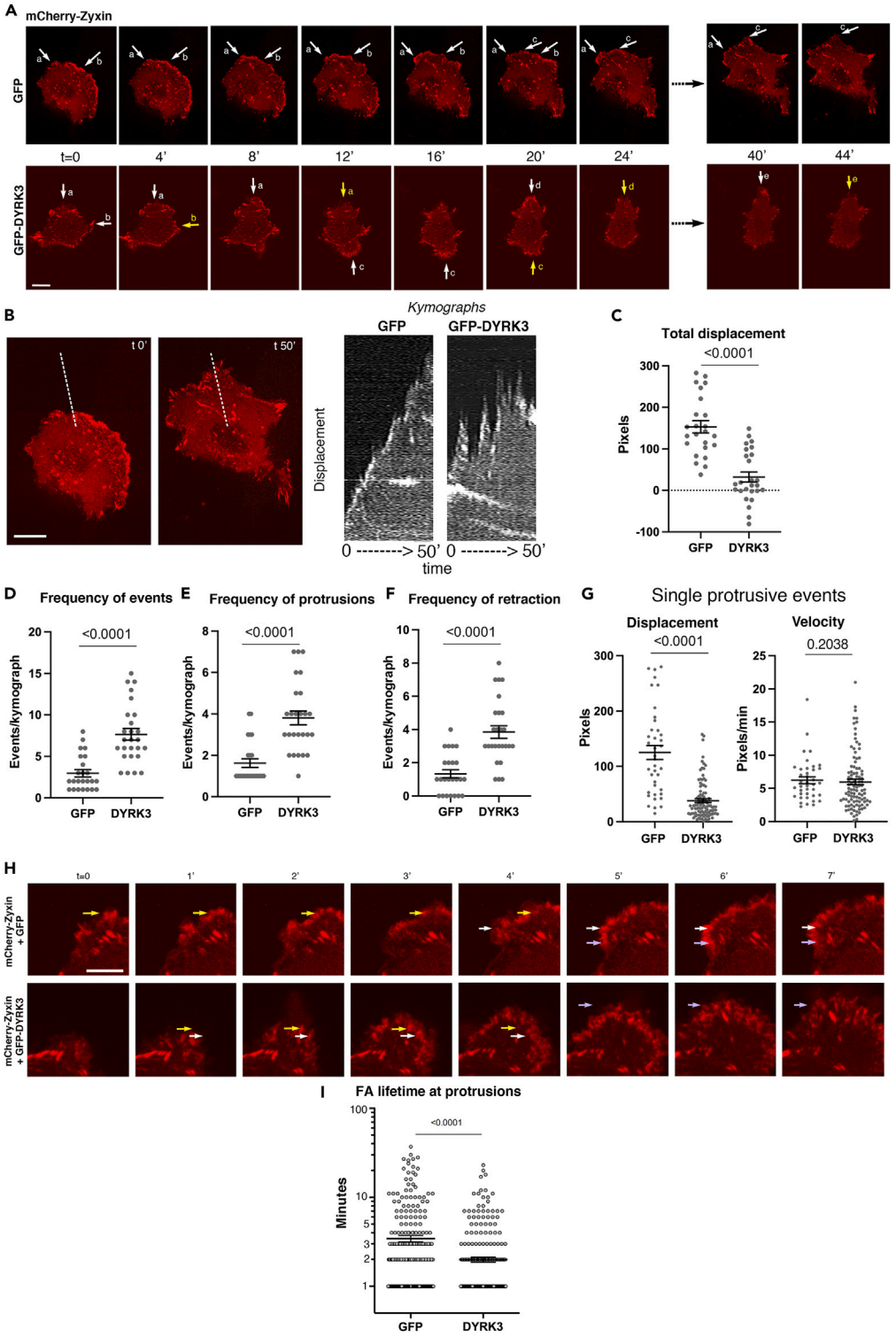

Figure 5. DYRK3 alters the protrusive activity and turnover of focal adhesions of cells migrating on fibronectin

MDA-MB-231 cells expressing the focal adhesion marker mCherry-Zyxin with either GFP or GFP-DYRK3 were plated on fibronectin-coated coverslips for migration, and recorded for 50 min at 1 frame/min.

(A) Frames from time-lapses of GFP- (top) and GFP-DYRK3-transfected cells (bottom). White arrows indicate protrusions, yellow arrows retractions. Each number refers to a single event.

Figure 5. *Continued*

(B) Example of kymographs (50 min recordings) used to analyze the dynamics of protrusion/retraction at the cell edge. Bars, 10 μm.

(C–G) Quantification (means ± SEM) of cell edge behavior at the protruding edge of transfected cells expressing either GFP or GFP-DYRK3 (DYRK3). (C) Total displacement of the protruding fronts of cells during 50 min recordings. (D-F) Frequency (number of events in kymographs during 50 min recording interval) of total (D), protrusive (E), and retractive (F) events (n = 24–26 kymographs from 14 cells, 3 experiments). (G) Displacement (left) and velocity (right) of single protrusive events; n = 39 (GFP) and 99 (GFP-DYRK3) events from 14 cells/sample (3 experiments).

(H) Frames from time lapses of cells expressing the indicated fluorescently tagged proteins. Colored arrows indicate different adhesions forming near the edge of motile MDA-MB-231 cells. Bar, 5 μm.

(I) Lifetime of mCherry-Zyxin-positive adhesions forming near the protruding edge of cells. Bars represent means ± SEM (n = 335–394 focal adhesions from 5 cells/sample; 2 experiments). Statistics: two-sided, unpaired t-test.

Liprin-α1 is phosphorylated in cells expressing increased levels of DYRK3

Liprin-α1 promotes the stability of lamellipodia: depletion of the endogenous protein affects their stability, while Liprin-α1 overexpression induces larger lamellipodia enhancing cell spreading on ECM.[16,17] The effects observed in migrating MDA-MB-231 cells after silencing endogenous Liprin-α1 are similar to those observed after DYRK3 overexpression, suggesting that the kinase may affect the stability of lamellipodia by inhibiting the function of Liprin-α1. We tested the hypothesis that PMAP proteins are substrates of the DYRK3 enzyme. We co-expressed either GFP or GFP-DYRK3 together with either LL5α, Liprin-α1, or ERC1 in COS7 cells and analyzed the cell lysates by immunoblotting. A clear partial shift of the Liprin-α1 band was observed only in lysates coexpressing GFP-DYRK3 with FLAG-Liprin-α1 (Figures 6A and 6B). Phosphorylation of Liprin-α1 in GFP-DYRK3 transfected cells was shown by incubating cell lysates for 30 min at 30°C with the λ phosphatase, which abrogated the higher molecular weight smear of Liprin-α1 (Figure 6B). Increased Liprin-α1 phosphorylation was not observed in cells co-expressing the kinase-dead mutant DYRK3^{K218M} (Figure 6C), and was confirmed by immunoprecipitation from lysates of cells co-transfected with Liprin-α1 and DYRK3 (Figure 6C). DYRK3 expression increased also the phosphorylation of endogenous Liprin-α1 in different cell types (Figures 6D and 6E) including MDA-MB-231 cells, where the increase was prevented by 2 h incubation with the GSK-626616, a small-molecule inhibitor of DYRK3[25] (Figure 6E).

A broader band smeared toward higher molecular weights and sensitive to treatment with the λ phosphatase was observed with the N-terminal half of Liprin-α1 (Figures 7A and 7B). To confirm the phosphorylation of the N-terminal Liprin(1–675), we analyzed cell lysates by immunoblotting after SDS–PAGE with a gel containing PhosTag, a compound that delays the migration of phosphorylated proteins compared to their non-phosphorylated equivalents.[31] Liprin(1–675) showed a band with reduced migration corresponding to increased phosphorylation in cell lysates from COS7 cells expressing GFP-DYRK3. After incubation of the lysate from cells expressing GFP-DYRK3 with λ phosphatase to dephosphorylate Liprin(1–675) *in vitro*, the higher molecular weight band disappeared, and Liprin(1–675) ran as a compact band migrating faster on the PhosTag gel compared to the Liprin(1–675) band observed in control lysate from cells expressing GFP (Figure 7C). This suggests that the higher band represents a population of Liprin(1–675) molecules with a higher level of phosphorylation induced by GFP-DYRK3. Incubation of cells for 2 h with GSK-626616, inhibited Liprin(1–675) phosphorylation in lysates of cells expressing GFP-DYRK3 (Figures 7D and 7E).

Liprin-α1 rescues the defect in cell spreading induced by DYRK3

The results indicate that increased levels of DYRK3 in cells affect cell motility and PMAPs formation by phosphorylating PMAP components, thus causing their disassembly with effects on cell motility. Since it is known that Liprin-α1 stabilizes lamellipodia in motile cells,[16,17] we tested whether increasing the cellular levels of Liprin-α1 could rescue the spreading defect induced by the increased levels of DYRK3. The projected area of cells co-expressing GFP-DYRK3 and FLAG-Liprin-α1 was increased compared to control cells co-expressing GFP-DYRK3 with FLAG-βGalactosidase, but was significantly lower compared to cells overexpressing FLAG-Liprin-α1 alone (Figures 8A and 8B). On the other hand, expression of the kinase-dead mutant DYRK3^{K218M} neither affected cell spreading, nor the increase in cell spreading induced by Liprin-α1 overexpression (Figures 8A and 8B). This result indicates a partial rescue of the inhibition of cell spreading induced by kinase–active DYRK3 when the cellular level of Liprin-α1 is increased, and suggests a reciprocal influence of the levels of the DYRK3 kinase and of the scaffold Liprin-α1 in regulating cell edge dynamics (Figure 8C).

DISCUSSION

Our data show that DYRK3 is required for tumor cell motility, and that altered levels of DYRK3 affect tumor cell migration and the formation of PMAPs. DYRK3 silencing impairs invasion and ECM degradation. Interestingly, increased DYRK3 levels also inhibit cancer cell motility. Moreover, DYRK3 overexpression inhibits PMAPs formation and the turnover of focal adhesions at lamellipodia. Comparative analysis by using wildtype and kinase-dead DYRK3 indicates that the specific effects of DYRK3 on cell motility are partially kinase-independent. In cells expressing increased levels of DYRK3 immunochemical analysis showed an evident and specific hyperphosphorylation of Liprin-α1 among the core PMAP scaffold components. Our results suggest that an equilibrium between Liprin-α1 and DYRK3 levels is required for the stabilization of lamellipodia and efficient motile behavior of tumor cells.

DYRKs have been implicated in the regulation of cytoskeletal organization. DYRK1A interacts with N-WASP and phosphorylates it, inhibiting Arp2/3–mediated actin polymerization.[32] Moreover, different DYRKs affect the growth of neuronal processes. In particular, DYRK3 but not its kinase-dead mutant increases dendritic branching although the underlying mechanism is unknown.[33] The knowledge on the role of different DYRK family members in tumor formation is fragmentary. DYRK2 has an ambiguous role being both pro- and

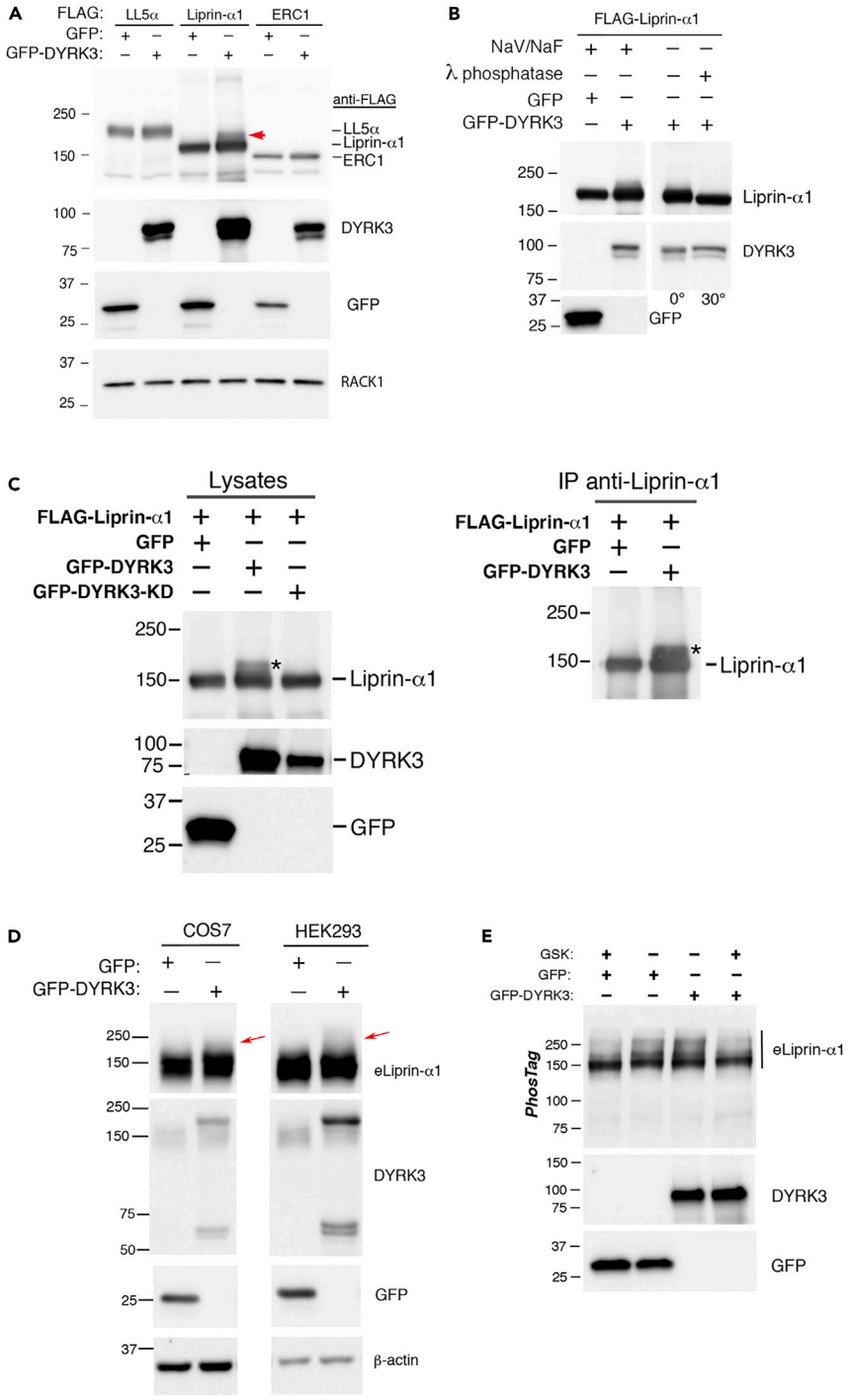

Figure 6. Increased phosphorylation of Liprin-α1 in cells overexpressing DYRK3

(A) COS7 cells co-expressing either GFP or GFP-DYRK3 with FLAG-LL5α, -Liprin-α1 or -ERC1 were lysed and analyzed by immunoblotting. A clear shift of part of the band corresponding to lower mobility (red arrowhead) induced by co-expression of DYRK3 was observed only for Liprin-α1. RACK1 used as loading control.

(B) Incubation with the λ phosphatase to eliminate phosphorylation increases the mobility of Liprin-α1.

(C) COS7 cells co-expressing GFP, GFP-DYRK3 or GFP-DYRK3^{K218M} with FLAG-Liprin-α1. A clear shift of part of the Liprin-α1 band was observed only in the presence of wild type DYRK3 (left). Immunoprecipitation (right) with anti-Liprin-α1 antibody of FLAG-Liprin-α1 from COS7 cells co-expressing either GFP or GFP-DYRK3. Immunoprecipitates (150 μg protein lysate/lane) and lysates (20 μg protein lysate/lane) were blotted with anti-FLAG (to detect FLAG-Liprin-α1), DYRK3, and GFP Abs.

Figure 6. *Continued*

(D) Phosphorylation of endogenous Liprin-α in COS7 and HEK293 cells expressing either GFP or GFP-DYRK3. Cells lysates analyzed by immunoblotting after PhosTag gel (10 μg protein lysate/lane loaded on 6% acrylamide gel with 25 μM PhosTag). Smear for lower mobility (red arrows) was enhanced by GFP-DYRK3 overexpression.

(E) MDA-MB-231 cells expressing either GFP or GFP-DYRK3 were incubated for 2 h with 1 μM of the DYRK3 inhibitor GSK-626616 (GSK +) or with control serum-free medium with DMSO (GSK –). Lysates were run on PhosTag SDS-PAGE (top filter: 10 μg protein lysate/lane loaded on 6% acrylamide gel with 25 μM PhosTag), or SDS-PAGE (middle and bottom filters: 30 μg protein lysate/lane loaded on 4–15% acrylamide gradient gels), and blotted to reveal endogenous Liprin-α1 (eLiprin-α1), GFP-DYRK3 and GFP.

anti-tumorigenic,[34] and less is known about DYRK3 and DYRK4 in cancer.[35] DYRK2 functions as a tumor suppressor by regulating cell survival, differentiation, proliferation and apoptosis.[22,36,37] Knockdown of DYRK2 expression promotes cancer cell invasion *in vitro* as well as tumorigenicity *in vivo*.[38] DYRK2 controls epithelial-mesenchymal transition in breast cancer and ovarian serous adenocarcinoma, and DYRK2 knockdown increases ovarian cancer cell invasion.[39] The ability of cell invasion and migration is abrogated by DYRK2-overexpression, and liver metastatic lesions were markedly diminished by ectopic expression of DYRK2, while patients whose liver metastases expressed low DYRK2 levels had significantly worse survival. The expression of the DYRK2 protein is significantly decreased in high-grade

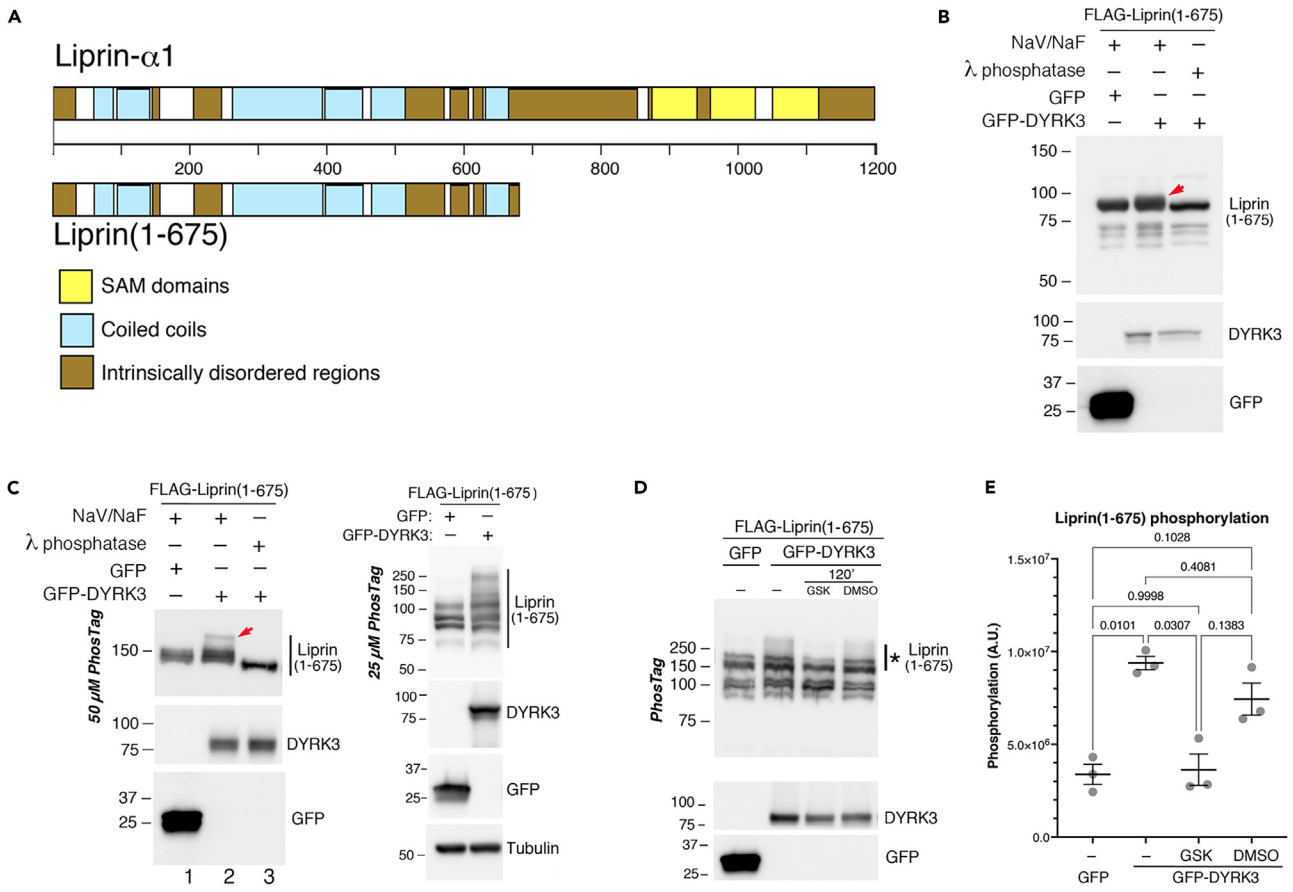

Figure 7. N-terminal region of Liprin-α1 contains phosphorylation sites regulated by DYRK3 enzymatic activity

(A) Scheme of Liprin-α1 and its N-terminal region Liprin(1–675).

(B) Lysates from COS7 cells co-transfected with either GFP or GFP-DYRK3 together with the N-terminal Liprin(1–675) fragment. Smear of the Liprin(1–675) band (red arrowhead) was observed only in lysates from cells co-expressing GFP-DYRK3, and was abolished by incubation with λ phosphatase.

(C) Left filters: phosphorylation of N-terminal Liprin(1–675) was detected by immunoblotting from PhosTag gels (7% acrylamide with 50 μM PhosTag) loaded with lysates from cells co-expressing Liprin(1–675) with either GFP (lane 1) or GFP-DYRK3 (lanes 2, 3). Sample in lane 3 was loaded after incubation with λ phosphatase. Right filters: enhanced resolution of DYRK3-induced phosphorylation of Liprin(1–675) after SDS-PAGE on 7% acrylamide gels supplemented with 25 μM PhosTag.

(D) Cotransfected COS7 cells analyzed by immunoblotting from 7% acrylamide gels supplemented with 25 μM PhosTag. Incubation for 2 h with 1 μM of the DYRK3 inhibitor GSK-626616 abolished phosphorylation of Liprin(1–675) induced by DYRK3 co-expression (asterisk).

(E) Quantification of the increased phosphorylation of Liprin(1–675) induced by DYRK3 (asterisk in panel D); mean ± SEM; n = 3 experiments. Brown-Forsythe and Welch ANOVA test with Dunnett's T3 posthoc.

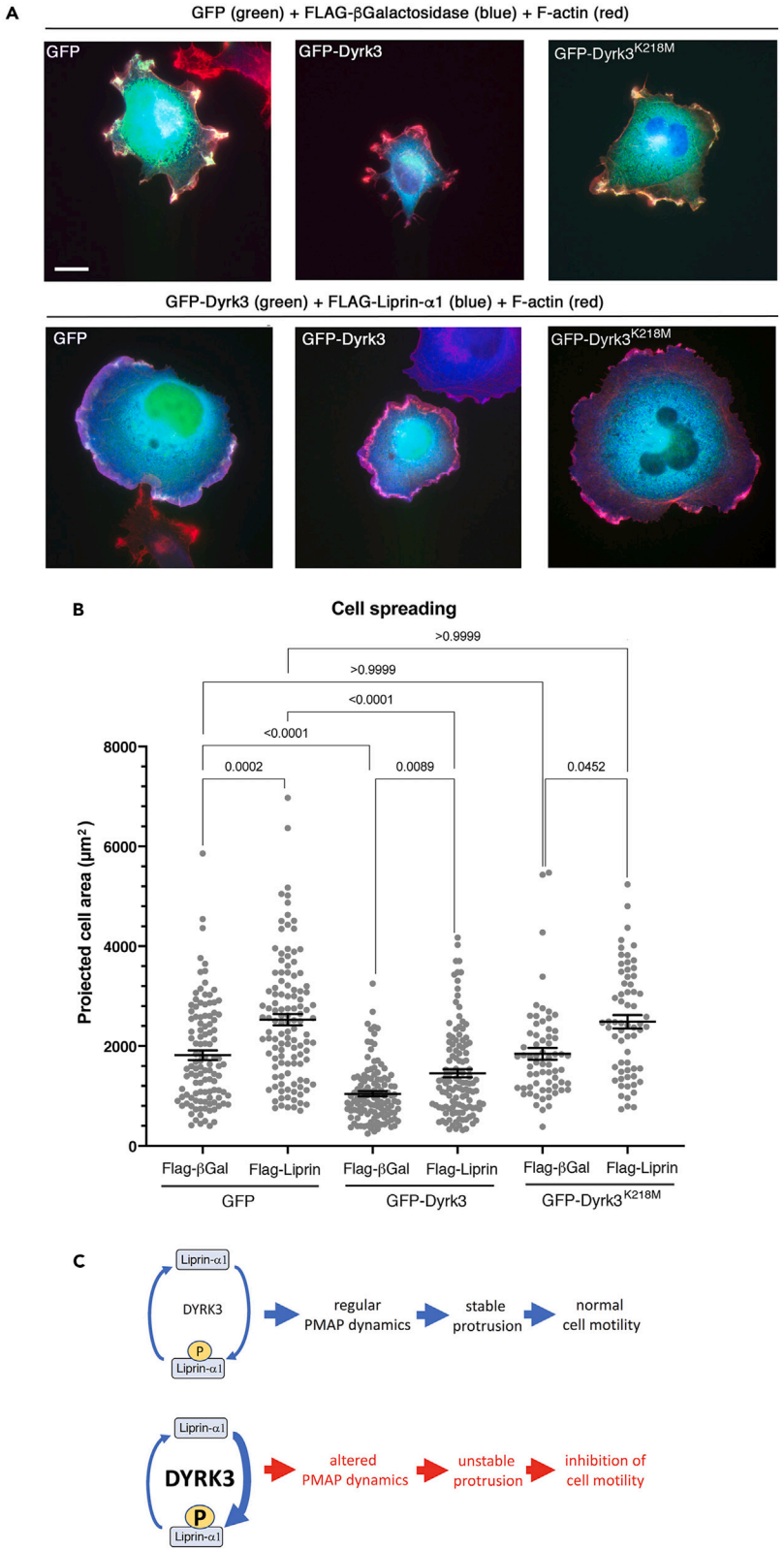
A
GFP (green) + FLAG-βGalactosidase (blue) + F-actin (red)
GFP
GFP-Dyrk3
GFP-Dyrk3K218M
GFP-Dyrk3 (green) + FLAG-Liprin-α1 (blue) + F-actin (red)
GFP
GFP-Dyrk3
GFP-Dyrk3K218M
B
Cell spreading
>0.9999
>0.9999
<0.0001
<0.0001
0.0002
0.0089
0.0452
Projected cell area (μm²)
8000
6000
4000
2000
0
Flag-βGal
Flag-Liprin
Flag-βGal
Flag-Liprin
Flag-βGal
Flag-Liprin
GFP
GFP-Dyrk3
GFP-Dyrk3K218M
C
Liprin-α1
DYRK3
P
Liprin-α1
regular
PMAP dynamics
stable
protrusion
normal
cell motility
Liprin-α1
DYRK3
P
Liprin-α1
altered
PMAP dynamics
unstable
protrusion
inhibition of
cell motility

Figure 8. Overexpression of PMAP protein Liprin-α1 rescues the inhibition of cell spreading induced by DYRK3

(A) COS7 cells transfected with the indicated constructs were plated for 1 h on fibronectin-coated coverslips (10 μg/mL) before fixation and immunofluorescence analysis. Bar, 20 μm.

(B) Quantification of the projected cell area (mean ± SEM; n = 64–119 cells). Statistic: One-way ANOVA Kruskal-Wallis test with Dunn's posthoc.

(C) Model for the proposed role of DYRK3 in regulating liprin-α1–promoted cell motility.

human gliomas, where low expression of DYRK2 has been related to poor prognosis. Accordingly, overexpression of DYRK2 in glioma cells inhibits transwell cell migration, while knockdown of DYRK2 promotes transwell migration.[40] While expression of the DYRK2 protein was undetectable in the MDA-MB-231 breast cancer cells used in the present study, we could detect endogenous DYRK3 in these invasive cells, while the same protein was undetected in other less invasive breast cancer cell lines (Figure S1A). The information on the role of DYRK3 in tumor cells is limited, and points to distinct roles and different effects in distinct types of tumors. DYRK3 inhibits hepatocellular carcinoma[41]; on the other hand DYRK3 is upregulated in neuroblastoma patients with poor prognosis,[42] and it promotes aggressiveness of glioblastoma,[43] with DYRK3 downregulation impairing glioblastoma cell migration and invasion. Here, we observed an inhibitory effect on tumor cell motility both after silencing endogenous DYRK3, or after overexpression of this kinase, suggesting that altering the levels of the kinase has deleterious effects on the motility of invasive MDA-MB-231 cells. Higher levels of expression of the kinase had clear inhibitory effects on the stability of lamellipodia, without affecting the ability *per se* of cells to form these structures (Figure 5). This effect was accompanied by a strong inhibition of the formation of PMAPs, and an evident increase of Liprin-α1 phosphorylation. We hypothesize that DYRK3 may influence the formation of PMAPs by regulating the ability of Liprin-α1 to assemble the protein network promoting cell motility at the cell edge (Figure 8C), with consequences both on the formation of PMAPs and on the formation and turnover of adhesions at the protruding cell edge.

Interestingly, recent studies indicate that DYRK3 regulates distinct biomolecular condensates originating from liquid-liquid phase separation (LLPS). LLPS has been shown to underlie the assembly of several types of membraneless biomolecular condensates in the cytoplasm and nucleus of cells,[44] but the molecular mechanisms controlling the dynamics of these condensates are poorly understood. In this direction, DYRK3 has been shown to couple the condensation and dissolution of stress granules to the signaling mediated by mechanistic target of rapamycin complex 1 (mTORC1): active DYRK3 allows stress granule dissolution to releases mTORC1 for signaling.[25] Moreover, in *C. elegans* embryos the DYRK homolog MBK-2 regulates the dynamics of P granules by phosphorylating the MEG proteins to induce P granule disassembly, while dephosphorylation of MEGs by the phosphatase PP2A promotes granule assembly.[26] Other examples include the regulation of the formation of different types of biomolecular condensates involved in mitosis by DYRK3–mediated phosphorylation.[23] These studies indicate that the activity of the DYRK3 kinase is essential to dissolve and condense several membraneless condensates during mitosis or cytoplasmic granule formation in response to specific functional needs of the cell. The concept may extend also to nuclear DYRK members: DYRK1A accumulates in nuclear speckles, biomolecular condensates involved in splicing, and induces their disassembly in a kinase–dependent mode.[45] Likewise, in this study we observed that PMAPs are regulated by DYRK3. Increased levels of DYRK3 but not of its kinase-dead mutant, inhibit the formation of endogenous cytoplasmic PMAPs (Figure 3), and interfere with cell spreading and motility by affecting the stability of lamellipodia (Figure 5), as observed after depletion of endogenous Liprin-α1,[16,17] which is required also for the formation of PMAPs (*8*). We previously observed that PMAPs show liquid–like behavior in migrating tumor cells, and suggested that they may form by LLPS.[46] In this direction, later studies have shown that Liprin-α proteins are implicated in the formation of condensates by LLPS at presynaptic sites in neuronal cells.[47,48] Phosphorylation/dephosphorylation cycles appear as an efficient way to rapidly regulate assembly/disassembly of protein networks involved in dynamic cellular processes as those occurring at the protruding edge of migrating cells.[49] It is expected that cell edge extension depends on the controlled condensation and dissolution driven by one or more internal components of the functional protein network. Given the role of Liprin-α1 both as a driver of PMAPs and a stabilizer of lamellipodia, it is expected that interfering with the precise timing of PMAPs turnover by altering Liprin-α1 phosphorylation may negatively influence the process of spreading and migration (Figure 8C). Our results highlight a mechanism regulating cell motility: future work is expected to expand the molecular details to help understanding the complex array of events required to coordinate cell movement.

DYRK3 is an established Ser/Thr kinase, and phosphopeptide analysis has led to the identification of consensus phosphorylation sequences for DYRK proteins; the consensus RXS/TP was suggested for DYRK3 (and DYRK2) kinases.[50] On the other hand, it has to be noted that not all phosphorylation sites identified match this consensus sequence.[19] The N-terminal region of Liprin-α1 includes putative consensus sites for DYRK3, although different phosphorylation sites by DYRK3 on Liprin-α1 can not be excluded at this time.

Intriguingly we found that DYRK3 depletion and overexpression have similar effects on cell motility. We would like to speculate that this may be due to the fact that cycles of phosphorylation/dephosphorylation events that regulate one or more aspects of cell motility (e.g., focal adhesion turnover, actin dynamics, and/or PMAPs assembly and disassembly) may be negatively affected not only by abolishing DYRK3 function, but also by excessive phosphorylation of important players involved in these dynamic processes.

Given the relevance observed for tumor cell invasion, further analysis of the mechanisms regulated by DYRK3 in motile cells may highlight molecular targets to interfere with tumor metastasis.

Limitations of the study

A limitation is the lack of experiments *in vivo* showing the effects of altering the expression of DYRK3 on invasion using an animal model.

STAR★METHODS

Detailed methods are provided in the online version of this paper and include the following:

- KEY RESOURCES TABLE
- RESOURCE AVAILABILITY
  - Lead contact
  - Materials availability
  - Data and code availability
- EXPERIMENTAL MODEL AND STUDY PARTICIPANT DETAILS
- METHOD DETAILS
  - Plasmids and siRNAs
  - Cell transfection
  - Biochemical analysis
  - Immunofluorescence
  - Functional analysis
  - Phosphatase treatment
  - PhosTag gels
  - Quantification of focal adhesions in COS7 cells
  - Analysis of focal adhesions in migrating MDA-MB-231 cells
  - Quantification of PMAPs near focal adhesions
  - Quantification of PMAPs at the leading edge of migrating MDA-MB-231 cells
  - Analysis of cell edge dynamics and focal adhesion lifetime in migrating cells
- QUANTIFICATION AND STATISTICAL ANALYSIS

SUPPLEMENTAL INFORMATION

Supplemental information can be found online at https://doi.org/10.1016/j.isci.2024.109440.

ACKNOWLEDGMENTS

We thank Dr. Mary Beckerle (University of Utah) for the anti-zyxin antibody, and dr. Sara Courtneidge (Oregon Health & Science University) for the mouse mAb for Src; the personnel of the Advanced Light and Electron Microscopy BioImaging Center (ALEMBIC) of the San Raffaele Scientific Institute, and dr. Matteo Brindisi for technical support. This study was supported by AIRC – Associazione Italiana per la Ricerca sul Cancro, grant IG 2023 ID 29097, and by the Italian Ministry of University and Research - PRIN 2022, grant 2022EMZJL4. M.R. was supported by the fellowship 24231 from AIRC; K.S. was supported by the fellowship 22253 from AIRC. The work performed by L.M.R. was supported by an FCSR-Fronzaroli fellowship, and was in partial fulfillment of the requirements for obtaining the PhD degree at the Vita-Salute San Raffaele University.

AUTHOR CONTRIBUTIONS

I.D.C. and M.R. conceived the project with the important input from A.K.R., L.P., and L.M.R.; M.R., L.M.R., K.S., and J.M.C. performed the functional and morphological analysis; L.M.R., M.R., S.S., and D.T. performed the biochemical and immunochemical analysis; I.D.C. and M.R. wrote the paper with input from all authors.

DECLARATION OF INTERESTS

The authors declare no competing interests.

Received: October 6, 2023
Revised: January 25, 2024
Accepted: March 4, 2024
Published: March 6, 2024

REFERENCES

1. Parsons, J.T., Horwitz, A.R., and Schwartz, M.A. (2010). Cell adhesion: integrating cytoskeletal dynamics and cellular tension. Nat. Rev. Mol. Cell Biol. *11*, 633–643. https://doi.org/10.1038/nrm2957.
2. Lappalainen, P., Kotila, T., Jégou, A., and Romet-Lemonne, G. (2022). Biochemical and mechanical regulation of actin dynamics. Nat. Rev. Mol. Cell Biol. *23*, 836–852. https://doi.org/10.1038/s41580-022-00508-4.
3. Astro, V., and de Curtis, I. (2015). Plasma membrane-associated platforms: dynamic scaffolds that organize membrane-associated events. Sci. Signal. *8*. https://doi.org/10.1126/scisignal.aaa3312.
4. Ramella, M., Ribolla, L.M., and de Curtis, I. (2022). Liquid-Liquid Phase Separation at the Plasma Membrane-Cytosol Interface: Common Players in Adhesion, Motility, and Synaptic Function. J. Mol. Biol. *434*, 167228. https://doi.org/10.1016/j.jmb.2021.167228.
5. Lansbergen, G., Grigoriev, I., Mimori-Kiyosue, Y., Ohtsuka, T., Higa, S., Kitajima, I.,

Demmers, J., Galjart, N., Houtsmuller, A.B., Grosveld, F., and Akhmanova, A. (2006). CLASPs attach microtubule plus ends to the cell cortex through a complex with LL5beta. Dev. Cell *11*, 21–32. https://doi.org/10.1016/j.devcel.2006.05.012.

6. van der Vaart, B., van Riel, W.E., Doodhi, H., Kevenaar, J.T., Katrukha, E.A., Gumy, L., Bouchet, B.P., Grigoriev, I., Spangler, S.A., Yu, K.L., et al. (2013). CFEOM1-associated kinesin KIF21A is a cortical microtubule growth inhibitor. Dev. Cell *27*, 145–160. https://doi.org/10.1016/j.devcel.2013.09.010.
7. Hotta, A., Kawakatsu, T., Nakatani, T., Sato, T., Matsui, C., Sukezane, T., Akagi, T., Hamaji, T., Grigoriev, I., Akhmanova, A., et al. (2010). Laminin-based cell adhesion anchors microtubule plus ends to the epithelial cell basal cortex through LL5alpha/beta. J. Cell Biol. *189*, 901–917. https://doi.org/10.1083/jcb.200910095.
8. Astro, V., Chiaretti, S., Magistrati, E., Fivaz, M., and de Curtis, I. (2014). Liprin-α1, ERC1 and LL5 define polarized and dynamic structures that are implicated in cell migration. J. Cell Sci. *127*, 3862–3876. https://doi.org/10.1242/jcs.155663.
9. Stehbens, S.J., Paszek, M., Pemble, H., Ettinger, A., Gierke, S., and Wittmann, T. (2014). CLASPs link focal-adhesionassociated microtubule capture to localized exocytosis and adhesion site turnover. Nat. Cell Biol. *16*, 561–573. https://doi.org/10.1038/ncb2975.
10. Sala, K., Raimondi, A., Tonoli, D., Tacchetti, C., and de Curtis, I. (2018). Identification of a membrane-less compartment regulating invadosome function and motility. Sci. Rep. *8*, 1164. https://doi.org/10.1038/s41598-018-19447-2.
11. Serra-Pagès, C., Medley, Q.G., Tang, M., Hart, A., and Streuli, M. (1998). Liprins, a family of LAR transmembrane protein-tyrosine phosphatase-interacting proteins. J. Biol. Chem. *273*, 15611–15620. https://doi.org/10.1074/jbc.273.25.15611.
12. Zhen, M., and Jin, Y. (1999). The liprin protein SYD-2 regulates the differentiation of presynaptic termini in *C. elegans*. Nature *401*, 371–375. https://doi.org/10.1038/43886.
13. Wyszynski, M., Kim, E., Dunah, A.W., Passafaro, M., Valtschanoff, J.G., Serra-Pagès, C., Streuli, M., Weinberg, R.J., and Sheng, M. (2002). Interaction between GRIP and liprin-alpha/SYD2 is required for AMPA receptor targeting. Neuron *34*, 39–52. https://doi.org/10.1016/s0896-6273(02)00640-2.
14. Xie, X., Liang, M., Yu, C., and Wei, Z. (2021). Liprin-α-Mediated Assemblies and Their Roles in Synapse Formation. Front. Cell Dev. Biol. *9*, 653381. https://doi.org/10.3389/fcell.2021.653381.
15. Pehkonen, H., de Curtis, I., and Monni, O. (2021). Liprins in oncogenic signaling and cancer cell adhesion. Oncogene *40*, 6406–6416. https://doi.org/10.1038/s41388-021-02048-1.
16. Asperti, C., Astro, V., Totaro, A., Paris, S., and de Curtis, I. (2009). Liprin-alpha1 promotes cell spreading on the extracellular matrix by affecting the distribution of activated integrins. J. Cell Sci. *122*, 3225–3232. https://doi.org/10.1242/jcs.054155.
17. Astro, V., Asperti, C., Cangi, M.G., Doglioni, C., and de Curtis, I. (2011). Liprin-α1 regulates breast cancer cell invasion by affecting cell motility, invadopodia and extracellular matrix degradation. Oncogene *30*, 1841–1849. https://doi.org/10.1038/onc.2010.562.
18. Lochhead, P.A., Sibbet, G., Morrice, N., and Cleghon, V. (2005). Activation-loop autophosphorylation is mediated by a novel transitional intermediate form of DYRKs. Cell *121*, 925–936. https://doi.org/10.1016/j.cell.2005.03.034.
19. Aranda, S., Laguna, A., and de la Luna, S. (2011). DYRK family of protein kinases: evolutionary relationships, biochemical properties, and functional roles. Faseb. J. *25*, 449–462. https://doi.org/10.1096/fj.10-165837.
20. Miyata, Y., and Nishida, E. (2021). Protein quality control of DYRK family protein kinases by the Hsp90-Cdc37 molecular chaperone. Biochim. Biophys. Acta Mol. Cell Res. *1868*, 119081. https://doi.org/10.1016/j.bbamcr.2021.119081.
21. Zhang, D., Li, K., Erickson-Miller, C.L., Weiss, M., and Wojchowski, D.M. (2005). DYRK gene structure and erythroid-restricted features of DYRK3 gene expression. Genomics *85*, 117–130. https://doi.org/10.1016/j.ygeno.2004.08.021.
22. Mimoto, R., Taira, N., Takahashi, H., Yamaguchi, T., Okabe, M., Uchida, K., Miki, Y., and Yoshida, K. (2013). DYRK2 controls the epithelial-mesenchymal transition in breast cancer by degrading Snail. Cancer Lett. *339*, 214–225. https://doi.org/10.1016/j.canlet.2013.06.005.
23. Rai, A.K., Chen, J.X., Selbach, M., and Pelkmans, L. (2018). Kinase-controlled phase transition of membraneless organelles in mitosis. Nature *559*, 211–216. https://doi.org/10.1038/s41586-018-0279-8.
24. Astro, V., Tonoli, D., Chiaretti, S., Badanai, S., Sala, K., Zerial, M., and de Curtis, I. (2016). Liprin-α1 and ERC1 control cell edge dynamics by promoting focal adhesion turnover. Sci. Rep. *6*, 33653. https://doi.org/10.1038/srep33653.
25. Wippich, F., Bodenmiller, B., Trajkovska, M.G., Wanka, S., Aebersold, R., and Pelkmans, L. (2013). Dual specificity kinase DYRK3 couples stress granule condensation/dissolution to mTORC1 signaling. Cell *152*, 791–805. https://doi.org/10.1016/j.cell.2013.01.033.
26. Wang, J.T., Smith, J., Chen, B.C., Schmidt, H., Rasoloson, D., Paix, A., Lambrus, B.G., Calidas, D., Betzig, E., and Seydoux, G. (2014). Regulation of RNA granule dynamics by phosphorylation of serine-rich, intrinsically disordered proteins in *C. elegans*. Elife *3*, e04591. https://doi.org/10.7554/eLife.04591.
27. Paradžik, M., Humphries, J.D., Stojanović, N., Nestić, D., Majhen, D., Dekanić, A., Samaržija, I., Sedda, D., Weber, I., Humphries, M.J., and Ambriović-Ristov, A. (2020). KANK2 Links αVβ5 Focal Adhesions to Microtubules and Regulates Sensitivity to Microtubule Poisons and Cell Migration. Front. Cell Dev. Biol. *8*, 125. https://doi.org/10.3389/fcell.2020.00125.
28. Kanchanawong, P., Shtengel, G., Pasapera, A.M., Ramko, E.B., Davidson, M.W., Hess, H.F., and Waterman, C.M. (2010). Nanoscale architecture of integrin-based cell adhesions. Nature *468*, 580–584. https://doi.org/10.1038/nature09621.
29. Nayal, A., Webb, D.J., Brown, C.M., Schaefer, E.M., Vicente-Manzanares, M., and Horwitz, A.R. (2006). Paxillin phosphorylation at Ser273 localizes a GIT1-PIX-PAK complex and regulates adhesion and protrusion dynamics. J. Cell Biol. *173*, 587–589. https://doi.org/10.1083/jcb.200509075.
30. Grande-García, A., Echarri, A., de Rooij, J., Alderson, N.B., Waterman-Storer, C.M., Valdivielso, J.M., and del Pozo, M.A. (2007). Caveolin-1 regulates cell polarization and directional migration through Src kinase and Rho GTPases. J. Cell Biol. *177*, 683–694. https://doi.org/10.1083/jcb.200701006.
31. Kinoshita, E., Kinoshita-Kikuta, E., Takiyama, K., and Koike, T. (2006). Phosphate-binding tag, a new tool to visualize phosphorylated proteins. Mol. Cell. Proteomics *5*, 749–757. https://doi.org/10.1074/mcp.T500024-MCP200.
32. Park, J., Sung, J.Y., Park, J., Song, W.J., Chang, S., and Chung, K.C. (2012). DYRK1A negatively regulates the actin cytoskeleton through threonine phosphorylation of N-WASP. J. Cell Sci. *125*, 67–80. https://doi.org/10.1242/jcs.086124.
33. Slepak, T.I., Salay, L.D., Lemmon, V.P., and Bixby, J.L. (2012). DYRK kinases regulate phosphorylation of doublecortin, cytoskeletal organization, and neuronal morphology. Cytoskeleton *69*, 514–527. https://doi.org/10.1002/cm.21021.
34. Tandon, V., de la Vega, L., and Banerjee, S. (2021). Emerging roles of DYRK2 in cancer. J. Biol. Chem. *296*, 100233. https://doi.org/10.1074/jbc.REV120.015217.
35. Lindberg, M.F., and Meijer, L. (2021). Dual-Specificity, Tyrosine Phosphorylation-Regulated Kinases (DYRKs) and cdc2-Like Kinases (CLKs) in Human Disease, an Overview. Int. J. Mol. Sci. *22*, 6047. https://doi.org/10.3390/ijms22116047.
36. Ito, D., Yogosawa, S., Mimoto, R., Hirooka, S., Horiuchi, T., Eto, K., Yanaga, K., and Yoshida, K. (2017). Dual-specificity tyrosine-regulated kinase 2 is a suppressor and potential prognostic marker for liver metastasis of colorectal cancer. Cancer Sci. *108*, 1565–1573. https://doi.org/10.1111/cas.13280.
37. Taira, N., Mimoto, R., Kurata, M., Yamaguchi, T., Kitagawa, M., Miki, Y., and Yoshida, K. (2012). DYRK2 priming phosphorylation of c-Jun and c-Myc modulates cell cycle progression in human cancer cells. J. Clin. Invest. *122*, 859–872. https://doi.org/10.1172/JCI60818.
38. Imawari, Y., Mimoto, R., Hirooka, S., Morikawa, T., Takeyama, H., and Yoshida, K. (2018). Downregulation of dual-specificity tyrosine-regulated kinase 2 promotes tumor cell proliferation and invasion by enhancing cyclin-dependent kinase 14 expression in breast cancer. Cancer Sci. *109*, 363–372. https://doi.org/10.1111/cas.13459.
39. Yamaguchi, N., Mimoto, R., Yanaihara, N., Imawari, Y., Hirooka, S., Okamoto, A., and Yoshida, K. (2015). DYRK2 regulates epithelial-mesenchymal-transition and chemosensitivity through Snail degradation in ovarian serous adenocarcinoma. Tumour Biol. *36*, 5913–5923. https://doi.org/10.1007/s13277-015-3264-y.
40. Shen, Y., Zhang, L., Wang, D., Bao, Y., Liu, C., Xu, Z., Huang, W., and Cheng, C. (2017). Regulation of Glioma Cells Migration by DYRK2. Neurochem. Res. *42*, 3093–3102. https://doi.org/10.1007/s11064-017-2345-2.
41. Ma, F., Zhu, Y., Liu, X., Zhou, Q., Hong, X., Qu, C., Feng, X., Zhang, Y., Ding, Q., Zhao, J., et al. (2019). Dual-Specificity Tyrosine Phosphorylation-Regulated Kinase 3 Loss Activates Purine Metabolism and Promotes Hepatocellular Carcinoma Progression.

Hepatology *70*, 1785–1803. https://doi.org/10.1002/hep.30703.

42. Uhl, K.L., Schultz, C.R., Geerts, D., and Bachmann, A.S. (2018). Harmine, a dual-specificity tyrosine phosphorylation-regulated kinase (DYRK) inhibitor induces caspase-mediated apoptosis in neuroblastoma. Cancer Cell Int. *18*, 82. https://doi.org/10.1186/s12935-018-0574-3.
43. Kim, K., Lee, S., Kang, H., Shin, E., Kim, H.Y., Youn, H., and Youn, B. (2021). Dual Specificity Kinase DYRK3 Promotes Aggressiveness of Glioblastoma by Altering Mitochondrial Morphology and Function. Int. J. Mol. Sci. *22*, 2982. https://doi.org/10.3390/ijms22062982.
44. Banani, S.F., Lee, H.O., Hyman, A.A., and Rosen, M.K. (2017). Biomolecular condensates: organizers of cellular biochemistry. Nat. Rev. Mol. Cell Biol. *18*, 285–298. https://doi.org/10.1038/nrm.2017.7.
45. Alvarez, M., Estivill, X., and de la Luna, S. (2003). DYRK1A accumulates in splicing speckles through a novel targeting signal and induces speckle disassembly. J. Cell Sci. *116*, 3099–3107. https://doi.org/10.1242/jcs.00618.
46. Sala, K., Corbetta, A., Minici, C., Tonoli, D., Murray, D.H., Cammarota, E., Ribolla, L., Ramella, M., Fesce, R., Mazza, D., et al. (2019). The ERC1 scaffold protein implicated in cell motility drives the assembly of a liquid phase. Sci. Rep. *9*, 13530. https://doi.org/10.1038/s41598-019-49630-y.
47. McDonald, N.A., Fetter, R.D., and Shen, K. (2020). Assembly of synaptic active zones requires phase separation of scaffold molecules. Nature *588*, 454–458. https://doi.org/10.1038/s41586-020-2942-0.
48. Emperador-Melero, J., Wong, M.Y., Wang, S.S.H., de Nola, G., Nyitrai, H., Kirchhausen, T., and Kaeser, P.S. (2021). PKC-phosphorylation of Liprin-α3 triggers phase separation and controls presynaptic active zone structure. Nat. Commun. *12*, 3057. https://doi.org/10.1038/s41467-021-23116-w.
49. de Curtis, I. (2021). Biomolecular Condensates at the Front: Cell Migration Meets Phase Separation. Trends Cell Biol. *31*, 145–148. https://doi.org/10.1016/j.tcb.2020.12.002.
50. Campbell, L.E., and Proud, C.G. (2002). Differing substrate specificities of members of the DYRK family of arginine-directed protein kinases. FEBS Lett. *510*, 31–36. https://doi.org/10.1016/s0014-5793(01)03221-5.
51. Ducut Sigala, J.L., Bottero, V., Young, D.B., Shevchenko, A., Mercurio, F., and Verma, I.M. (2004). Activation of transcription factor NF-kappaB requires ELKS, an IkappaB kinase regulatory subunit. Science *304*, 1963–1967. https://doi.org/10.1126/science.1098387.
52. Asperti, C., Pettinato, E., and de Curtis, I. (2010). Liprin-alpha1 affects the distribution of low-affinity beta1 integrins and stabilizes their permanence at the cell surface. Exp. Cell Res. *316*, 915–926. https://doi.org/10.1016/j.yexcr.2010.01.017.
53. Artym, V.V., Zhang, Y., Seillier-Moiseiwitsch, F., Yamada, K.M., and Mueller, S.C. (2006). Dynamic interactions of cortactin and membrane type 1 matrix metalloproteinase at invadopodia: defining the stages of invadopodia formation and function. Cancer Res. *66*, 3034–3043. https://doi.org/10.1158/0008-5472.CAN-05-2177.

STAR★METHODS

KEY RESOURCES TABLE

REAGENT or RESOURCE	SOURCE	IDENTIFIER
Antibodies		
Calnexin, mouse monoclonal antibody	BD Transduction	610523
DYRK2, mouse monoclonal antibody	R&D Systems	MAB5408
DYRK3, goat polyclonal antibody	R&D Systems	AF5409
DYRK4, mouse monoclonal antibody	Santa Cruz Biotechnology	sc-390973
ERC1, mouse monoclonal antibody	Abcam	ab50312
ERC1, rabbit polyclonal antibody	Sigma-Aldrich	HPA019513
FLAG M2, mouse monoclonal antibody	Sigma-Aldrich	F1804
FLAG, rabbit polyclonal antibody	Sigma-Aldrich	F7425
GFP, chicken polyclonal antibody	Abcam	ab13970
GFP, rabbit polyclonal antibody	Invitrogen	A11122
Liprin-α1, mouse monoclonal antibody	Santa Cruz Biotechnology	sc-376141
Liprin-α1, rabbit polyclonal antibody	Proteintech	14175-1-AP
Paxillin, mouse monoclonal antibody	BD Transduction	610052
Paxillin, rabbit polyclonal antibody	GeneTex	GTX125891
Phosphotyrosine mouse monoclonal antibody	BD Transduction	P610000
RACK1, mouse monoclonal antibody	Santa Cruz Biotechnology	Sc-17754
Src cl.327, mouse monoclonal	S.Courtneidge	N/A
Talin, rabbit polyclonal antibody	Sigma-Aldrich	T 3287
Zyxin cl B38, rabbit polyclonal antibody	Mary C. Beckerle, Univ.Utah	N/A
Zyxin, mouse monoclonal antibody	Synaptic Systems	307011
α-Tubulin, mouse monoclonal antibody	Sigma-Aldrich	T9026
β-Actin, rabbit polyclonal antibody	Abcam	Ab8227
Anti-rabbit IgG HRP	Jackson	111-035-144, WB 1:5000
Anti-mouse IgG HRP	Jackson	115-035-003, WB 1:5000
Anti-goat IgG HRP	R&D Systems	HAF017, WB 1:1000
Anti-mouse Alexa Fluor 488	Thermo Scientific	A21202, IF 1:200
Anti-mouse IgG1 Alexa Fluor 568	Thermo Scientific	A21124, IF 1:200
Anti-mouse Alexa Fluor 546	Thermo Scientific	A10036, IF 1:200
Anti-mouse Alexa Fluor 647	Thermo Scientific	A31571, IF 1:200
Anti-rabbit Alexa Fluor 488	Thermo Scientific	A11008, IF 1:200
Anti-rabbit Alexa Fluor 488	Thermo Scientific	A21206, IF 1:200
Anti-rabbit Alexa Fluor 568	Thermo Scientific	A10042, IF 1:200
Anti-rabbit Alexa Fluor 647	Thermo Scientific	A31573, IF 1:200
Anti-chicken Alexa Fluor 488	Thermo Scientific	A11039, IF 1:200
Anti-goat Alexa Fluor 546	Thermo Scientific	A11056, IF 1.200
Chemicals, peptides, and recombinant proteins		
GSK-626616, small molecule DYRK3 inhibitor	Tocris Bioscience	CID: 15981157
Alexa Fluor 568 Phalloidin	Thermo Scientific	A12380
Alexa Fluor 647 Phalloidin	Thermo Scientific	A22287

(*Continued on next page*)

Continued

REAGENT or RESOURCE	SOURCE	IDENTIFIER
Deposited data		
Raw and analyzed data at: https://ordr.hsr.it/research-data/	This paper	https://doi.org/10.17632/95pgfjvvzp.1
Oligonucleotides		
siRNA sequence DYRK3-a: 5′CGGAUUUUGGAGCAUCUUAUU3′	Carlo Erba Reagents	N/A
siRNA sequence DYRK3-b: 5′CCAUCUAGCUUAUCGAUAUUU3′	Carlo Erba Reagents	N/A
siRNA sequence DYRK3-c: 5′GAAAAGACAUGGAGUUAUUUU3′	Carlo Erba Reagents	N/A
siRNA sequence DYRK2.1: 5′GGUGCUAUCACAUCUAUAUUU3′	Carlo Erba Reagents	N/A
siRNA sequence DYRK2.2: 5′GGACAGUGCUCACGACACAUU 3′	Carlo Erba Reagents	N/A
siRNA sequence (Ctrl, Luciferase) 5′ CAUCACGUACGCGGAAUACUU 3′	Carlo Erba Reagents	N/A
siRNA sequence Liprin-α1 #1: 5′CCAAGGUACAAACUCUUAAUU 3′	Carlo Erba Reagents	N/A
siRNA sequence Liprin-α1 #2: 5′CGAGGUUGGUCAUGAAAGAUU 3′	Carlo Erba Reagents	N/A
Software and algorithms		
GraphPad Prism 9.0	GraphPad Software	https://www.graphpad.com
ImageJ	National Institutes of Health	https://imagej.net/ij/

RESOURCE AVAILABILITY

Lead contact

Further information and requests for resources and reagents should be directed to and will be fulfilled by the lead contact, Ivan de Curtis (decurtis.ivan@hsr.it).

Materials availability

Further information and requests for materials should be directed to and will be fulfilled by the Principal Investigator, Dr. Ivan de Curtis (decurtis.ivan@hsr.it).

Data and code availability

All figures listed have associated raw data: microscopy and immunoblotting images, and data for graphs supporting the results presented in this study are available as of the date of publication in the San Raffaele Open Research Data Repository (ORDR, https://ordr.hsr.it/research-data/) with https://doi.org/10.17632/95pgfjvvzp.1.

Any additional information required to reanalyze the data reported in this paper is available from the lead contact author upon request.

EXPERIMENTAL MODEL AND STUDY PARTICIPANT DETAILS

Cell lines used in the study: COS7; MCF-7; HEK293; HeLa; T-47D; BT-474; MDA-MB-231 from ATCC. MDA-MB-231 and MCF-7 cells were grown in DMEM/F12 1:1 with 10% fetal bovine serum (FBS), 100 U/ml penicillin, 100 μg/mL streptomycin, 20 mM glutamine. COS7 cells were cultured in DMEM with 10% fetal clone III (Hyclone), 100 U/ml penicillin, 100 μg/mL streptomycin, 20 mM glutamine. HEK293, HeLa and BT-474 cells were cultured in DMEM with 10% FBS, 100 U/ml penicillin, 100 μg/mL streptomycin, 20 mM glutamine. T-47D cells were cultured in RPMI with 10% FBS, 100 U/ml penicillin, 100 μg/mL streptomycin, 20 mM glutamine. All cell lines used were negative for mycoplasma contamination.

METHOD DETAILS

Plasmids and siRNAs

SiRNAs

A pool of three siRNAs (Carlo Erba Reagents) was used to silence DYRK3 (100 nM total): DYRK3-a, DYRK3-b, DYRK3-c. A pool of two siRNAs (Carlo Erba Reagents) was used to silence DYRK2 (100 nM total): DYRK2.1 and DYRK2.2. SiRNAs for luciferase (Ctrl) and for Liprin-α1 (Liprin-α1#1 and Liprin-α1#2) were as described.[5,7,8,17,51]

Plasmids

GFP-tagged constructs including human DYRK2, DYRK3, DYRK3^{K218M} and DYRK4 were as described.[25] Liprin-α1 fragments Liprin(1–675) was cloned in pFLAG as described.[52]

Cell transfection

Transient transfections were performed 24 h after seeding cells on plastic or round 13–24 mm diameter glass coverslips using lipofectamine-2000 (Thermo Fisher Scientific, Paisley, UK) and the indicated siRNA (50–100 nM) and/or plasmid (1–6 μg of DNA). Transfection medium (OptiMEM) was replaced by growth medium 3.5–4 h after transfection. Cells transfected with plasmids were processed 24–48 h after transfection, while for siRNAs (alone or in combination with plasmids) cells were processed 48 h after transfection.

Biochemical analysis

Cells cooled on ice were washed twice with of ice-cold TBS (150 mM NaCl, 20 mM Tris-HCl pH 7.5), and lysed with 50–150 μL of lysis buffer (0.5% Triton X-100, 150 mM NaCl, 20 mM Tris-Cl pH 7.5, 1 mM NaV, 10 mM NaF, anti-proteases Complete 1× (Roche), 0.5 mM PMSF (Sigma-Aldrich) and 1 mM DTT). After 15 min at 4°C with rotation or vortexing every 5 min, insoluble material was removed by 16000 RCF centrifugation for 10 min at 4°C. Protein concentration in lysates was determined by the Bradford protein assay (Bio-Rad). For immunoprecipitation cell lysates were incubated with Protein-A–Sepharose beads (Cytiva) conjugated to antibody before processing for SDS-PAGE. For immunoblotting, lysates were separated by SDS-PAGE and transferred to 0.45 μm PROTRAN nitrocellulose membranes (GE Healthcare Amersham Biosciences). Membranes blocked in 5% (w/v) milk diluted in TBST were incubated with primary antibodies, HRP-conjugated secondary antibodies and revealed by Clarity with ChemiDoc MP Imaging System (Bio-Rad). Quantification of protein levels was done with ImageLab software (Bio-Rad).

Immunofluorescence

Transfected cells were fixed for 10–15 min at room temperature in 3% paraformaldehyde in PBS. After two washes, paraformaldehyde was blocked with 50 mM NH_4Cl. Then, cells were permeabilized with 0.1% Triton X-100 in PBS and blocked with 0.2% gelatin in PBS. Coverslips were then incubated with primary antibodies for 2 h at room temperature, washed, incubated with secondary antibodies for 45 min, and mounted with ProLong Gold antifade mounting solution (Thermo Fisher Scientific).

Functional analysis

For cell spreading on fibronectin, MDA-MB-231 or COS7 cells were transfected with the indicated plasmid and/or siRNA. After one day, cells ($5x10^4$ or $1x10^5$ cells/coverslip) were replated on human fibronectin–coated glass coverslips (fibronectin from Corning, 10 μg/mL, overnight at 4°C), and fixed after 18 h (MDA-MB-231) or 1 h culture (COS7). After immunofluorescence, cells were imaged at a Zeiss Axio Observer.Z1 inverted microscope with 63x lens equipped with Hamamatsu 9100 - 02 EM CCD Camera and Plan-Apochromat 63x (NA 1.4) lens. The projected cell area was quantified by ImageJ software (NIH, Bethesda, MD).

For random cell migration, MDA-MB-231 cells were plated, transfected, replated and acquired as described.[17] Briefly, 5×10^4 cells were seeded overnight on 2.5 μg/mL fibronectin-coated 6-well plate before time lapse for 5 h (one frame every 10 min) with IncuCyte Live-Cell Imaging System equipped with 10× lens (Essen BioScience, Ann Arbor, MI). Mean velocity was evaluated during 290 min recording with ImageJ (plugins Manual tracking and Chemotaxis tool). Cells undergoing division and non-moving cells were ignored.

For Matrigel invasion assays, MDA-MB-231 cells transfected for 48 h with the indicated siRNAs were seeded on 0.125 mg/mL Matrigel–coated transwells (8 μm pores, polycarbonate membrane, Millipore or Corning) in DMEM 0.1% BSA (1×10^5 cells in 100 μL/transwell), with lower chambers filled with NIH 3T3-conditioned medium (+stimulus) to stimulate invasion, while in control samples (no stimulus) lower chambers were filled with unconditioned medium. After 5 h of incubation at 37°C non-invading cells were removed from the upper side with a cotton swab, and cells invading the membranes were fixed with PFA and stained with DAPI for quantification.

For ECM degradation, MDA-MB-231 cells transfected with the indicated siRNAs and/or plasmid were re-plated (5×10^4 or 1×10^5 cells of complete medium per well with 15 mm coverslip insert) on coverslips coated with gelatin from pig skin (Oregon Green 488-conjugated, Life Technologies) diluted 1:4 in 0.2% gelatin in PBS and additionally coated with 10 μg/mL fibronectin for 1 h at 37°C.[10,17,53] After 5 h of incubation at 37°C cells were fixed and immunostained with appropriate primary and secondary antibodies or fluorescent phalloidin. Transfected cells were acquired with Axio Observer.Z1 63×. The dark areas of gelatin degradation and the projected cell areas were quantified by ImageJ on thresholded images.

Phosphatase treatment

Cells were lysed on ice in lysis buffer without phosphatase inhibitors. Dephosphorylation assays were performed with 5 units of l protein phosphatase (P0735S, New England Biolabs) per μg of protein lysate in 1× L phosphatase buffer (New England Biolabs buffer for protein metallophosphatases with $MnCl_2$), and incubated for 30 min at 30°C. Dephosphorylated samples were then separated by SDS-PAGE.

PhosTag gels

Transfected cells were lysed and lysates were spun for 15 min at 16,000 RCF at 4°C. Untreated and phosphatase-treated cleared lysates (10 μg/lane) were denatured for 10 min at 70°C in 2× LDS buffer (Invitrogen), and run on PhosTag gels (7% acrylamide with 25–50 μM PhosTag, 100 μM $Zn(NO_3)_2$, PhosTag from Wako Chemicals, Japan) in running buffer (50 mM MOPS, 50 mM Tris Base, 0.1% SDS, 5 mM sodium bisulfite, pH 7.8). Gels were washed twice for 30 min each in transfer buffer with 1 mM EDTA (1×NuPAGE Transfer Buffer, Invitrogen) for transfer overnight at 4°C to nitrocellulose membranes (Amersham) in 1×NuPAGE Transfer Buffer with 10% methanol, 5 mM sodium bisulfite. Membranes were then processed for immunoblotting.

Quantification of focal adhesions in COS7 cells

Cells with similar levels of the indicated transfected GFP-tagged proteins were analyzed using either a PerkinElmer UltraViewers spinning disk microscope, or a Leica TCS SP5 laser scanning confocal microscope equipped with 63× lens. Quantification of central and peripheral focal adhesions was performed in transfected COS7 cells fixed after 1 h spreading at 37°C on glass coverslips coated with fibronectin (10 μg/mL). The contrast of selected central areas of the cells were uniformly adjusted, and a fixed threshold was applied to detect focal adhesions and measure their areas with ImageJ. Objects larger than 0.17 μm^2 were considered. The density of peripheral focal adhesions was quantified on 1–μm–wide segments of the cell edge after uniform adjustment of the contrast. A fixed threshold was applied to measure the total area of focal adhesions within the cell edge segment. The density of peripheral focal adhesions was calculated as the ratio between the total focal adhesion area and the total area of the selected segment.

Analysis of focal adhesions in migrating MDA-MB-231 cells

MDA-MB-231 cells, plated at low density on fibronectin-coated (2.5 μg/mL) coverslips were transfected with GFP, GFP-DYRK3, or GFP-$DYRK3^{K218M}$. After 24h cells were fixed and immunostained for GFP, endogenous zyxin, paxillin, and talin. Cells were kept in PBS for acquisitions by a TIRF Leica SR GSD 3D TIRF microscope equipped with a 160× lens. TIRF angle (110 nm) and laser intensities were kept constant for all samples. Cells with similar GFP overexpression levels were analyzed as follows: the area occupied by focal adhesions (FA area/cell) was detected by immunostaining for endogenous paxillin, zyxin, or talin, and was evaluated on thresholded images using ImageJ. Values of FA area/cell area were presented as percentages of the total projected cell area (detected by GFP).

Quantification of PMAPs near focal adhesions

COS7 cells were transfected with GFP-tagged proteins. After 24 h cells were replated on glass coverslips coated overnight at 4°C with 10 μg/mL fibronectin. After 1 h spreading, cells were fixed and immunostained for GFP, endogenous paxillin and endogenous PMAP proteins (Liprin-α1 or ERC1). Cells with similar GFP expression levels were analyzed as follows: 2–3 internal areas per cell (cell edges excluded) including 3–10 focal adhesions/area were selected based on the signal of the endogenous PMAP protein (Liprin-α1 or ERC1). In each selected region we measured the area of focal adhesions and the volume of the endogenous PMAP protein (determined as the integrated density of the signal above a fixed threshold) using the ImageJ software. PMAP dynamics in living cells was followed in MDA-MB-231 cells triple–transfected with siRNA (control of DYRK3), GFP-ERC1, and mCherry-Lifeact. Images were collected 48 h after transfection in a controlled stage incubator (Oko-Lab) with a Leica TCS SP8 SMD FLIM confocal microscope equipped with HC PL APO CS2 100x lens (NA 1.4) and adaptive focus control.

Quantification of PMAPs at the leading edge of migrating MDA-MB-231 cells

Cells were transfected with GFP-tagged constructs or cotransfected GFP and siRNAs. After 24–48 h the cells were fixed and immunostained for GFP, endogenous PMAP proteins (Liprin-α1 or ERC1) and phalloidin. The quantification of the accumulation of Liprin-α1 and ERC1 near lamellipodia was performed as follows: lamellipodia were identified as cellular extensions with a clear F-actin-positive edge. We counted the number of lamellipodia positive for PMAPs (detected by the presence of clusters of either Liprin-α1 or ERC1) and the number of total lamellipodia in several cells for each experimental condition. We calculated the percentage of PMAP-positive lamellipodia for each experimental condition, and repeated this analysis for at least three independent experiments.

Analysis of cell edge dynamics and focal adhesion lifetime in migrating cells

MDA-MB-231 cells co-transfected with either GFP or GFP-DYRK3 and mCherry-Zyxin were replated after overnight culture on 35 mm diameter fibronectin-coated (2.5 μg/mL o.n. at 4°C) glass bottom dishes (MatTek Corporation) and recorded 16–21 h after replating. For imaging cells were supplied with phenol red-free DMEM medium with 10% FBS (Thermo Scientific). Images were acquired with 100X oil immersion objective for 50 min at 1 frame/min at 37°C and 5% CO_2 with with a Nikon CSU-X1 Spinning Disk, Nikon TE2 inverted microscope with a 100x oil lens (1.4 NA) and an ORCA-Flash 4.0 camera (Hamamatsu) with NIS Elements acquisition software (Nikon). The quantification of

cell edge dynamics was performed by kymographs using the Multiple Kymograph plugin (ImageJ). Briefly, kymographs were created by tracing a 400 pixel long and 1 pixel wide line perpendicular along the direction of lamellipodia growth over time. Total width of kymographs represents 50 min. Kymographs were analyzed to determine: (a) the displacement and relative average velocity of each event of cell edge extension or retraction; (b) the total displacement and relative average velocity during the 50 min interval of recording; (c) the frequency of the events obtained by counting the number of extension and retraction events. The same samples were also analyzed to measure the lifetime of focal adhesions at dynamic cell edges, which was conducted as reported.[30] Briefly, we evaluated the lifetime of individual or small groups of mCherry-Zyxin–positive focal adhesions near the dynamic protruding cell edges with ImageJ. Data are presented as means ± SEM; 25–26 kymographs from 14 to 15 cells per condition were analyzed.

QUANTIFICATION AND STATISTICAL ANALYSIS

Statistical analysis was performed using GraphPad Prism 9.0. All datasets were tested for normality using Shapiro-Wilk test. For datasets with normal distribution, the statistical significance was calculated using unpaired two-tailed Student's *t* test or one-way ANOVA with Dunnett's or Tukey's post-hoc. For datasets with nonnormal distribution, the statistical significance was calculated using Kruskal-Wallis test with Dunn's post-hoc. Data are presented as mean ± SEM.